

Dynamics of Excited Electrons in Copper and Ferromagnetic Transition Metals: Theory and Experiment

R. Knorren* and K.H. Bennemann

Institut für Theoretische Physik, Freie Universität Berlin, Arnimallee 14, 14195 Berlin, Germany

R. Burgermeister

Laboratorium für Festkörperphysik, ETH Zürich, 8093 Zürich, Switzerland

M. Aeschlimann†

Laboratorium für Technische Chemie, ETH Zürich, 8092 Zürich, Switzerland

(February 5, 2020)

Both theoretical and experimental results for the dynamics of photoexcited electrons at surfaces of Cu and the ferromagnetic transition metals Fe, Co, and Ni are presented. A model for the dynamics of excited electrons is developed, which is based on the Boltzmann equation and includes effects of photoexcitation, electron-electron scattering, secondary electrons (cascade and Auger electrons), and transport of excited carriers out of the detection region. From this we determine the time-resolved two-photon photoemission (TR-2PPE). Thus a direct comparison of calculated relaxation times with experimental results by means of TR-2PPE becomes possible. The comparison indicates that the magnitudes of the spin-averaged relaxation time τ and of the ratio $\tau_{\uparrow}/\tau_{\downarrow}$ of majority and minority relaxation times for the different ferromagnetic transition metals result not only from density-of-states effects, but also from different Coulomb matrix elements M . Taking $M_{\text{Fe}} > M_{\text{Cu}} > M_{\text{Ni}} = M_{\text{Co}}$ we get reasonable agreement with experiments.

I. INTRODUCTION

The dynamics of excited electrons at metal surfaces has been studied intensively over the last few years. It is of high interest both from the fundamental and the applied point of view. On the fundamental side it is of interest to understand the dynamics of non-equilibrium electrons in different metals on a femtosecond timescale. On the applied side excited-electron dynamics is, for example, an important topic for stimulated chemical reactions on surfaces. Hot electrons in the substrate can transfer energy to adsorbates on the surface and stimulate reactions. This effect could be used to control reactions on surfaces via excited electrons in the substrate, created by means of suitably chosen laser pulses. From the relaxation of hot electrons one may also learn about the decay of transient magnetization and of spin-selective transport and tunneling.

For these reasons, the substrate electron dynamics, the time evolution and energy distribution of excited electrons on metal surfaces after optical excitation, has been studied recently. Short laser pulses and the pump-probe technique have made possible the study of electronic dynamics on ultrashort timescales comparable to typical electron-electron interaction timescales. In metals lifetimes of excited electrons with excitation energies of about 1–2 eV above the Fermi energy are of the order of 5–50 fs, while typical laser pulses employed in this kind of experiment have widths of 15–50 fs. For electronic lifetimes of the order of the duration of the laser pulse, relaxation is present during the laser pulse itself.

The experimental technique of two-photon photoemission (2PPE) is a valuable tool for the study of excited-electron dynamics since it provides both time and energy resolution. Most 2PPE experiments aim at studying the relaxation of single excited electrons. The interpretation of the experimental results is made difficult by the fact that in many cases, one does not only observe single excited electrons but the effects of the whole distribution of excited electrons. A relaxation time is extracted from the width of the 2PPE signal as a function of the delay time between two laser pulses. The interpretation of this relaxation time has become more and more complicated with time. In the earlier experiments,^{1,2} the relaxation time was interpreted as the lifetime of a single excited electron under the influence of the Coulomb interaction. It was compared to the theoretical result for the lifetime of excited electrons in Fermi-liquid theory.³ The order of magnitude and the energy dependence of the lifetime calculated in Fermi-liquid theory was in good agreement with the experimentally determined relaxation time.^{1,2,4,5} However, it was soon realized that additional physical effects come into play, which have to be taken into account in an interpretation of the experimental data. The importance of the transport of excited electrons out of the detection region and of the

secondary-electron cascade was noted.^{1,4,6} It was pointed out that in 2PPE one generally observes the relaxation of a nascent photoexcited electron population and not only the lifetime of a single excited electron which can be compared with Fermi liquid theory. For low excitation energies, when electronic lifetimes are longer than a few tens of fs, ballistic transport is a mechanism which leads to a removal of electrons out of the probed region. In an experiment, this effect is indistinguishable from a stronger electronic decay. Furthermore, it was found that under certain conditions, the measured lifetime is non-monotonous and depends on the photon energy of the exciting laser.^{7–9} Both effects cannot be explained by a single-electron lifetime and transport. It has been pointed out that in addition to the excited electrons, the holes left behind in the excitation can influence the observed relaxation time of hot electrons.^{9,10} One explanation proposed was that secondary electrons generated by the filling of holes (Auger electrons) are responsible for the non-monotonous behavior in the observed lifetime.⁹ However, the contribution of Auger electrons to the relaxation time has raised some controversy. Petek *et al.* have argued that Auger electrons do not make an important contribution to the observed 2PPE signal and relaxation time at high intermediate-state energies $E - E_F > 1.5 - 2$ eV.^{11,12}

The $3d$ transition metals have not been as intensely studied as the noble metals. However, they offer several interesting features which make it worth to be studied in detail. To begin with, the ferromagnetic transition metals offer the opportunity to study spin-dependent interactions if the spin of the emitted electrons is measured.^{13,14} Furthermore, in case of transition metals, the closeness of the d bands to the Fermi energy makes it possible to study electronic interactions not only for free-electron-like states, but also for the more localized d -electron states.

On the theoretical side, the effect of the density of states on the lifetime and the influence of secondary electrons in photoemission from transition metals have been addressed by Penn *et al.*¹⁵ Using a similar approach, Zarate *et al.*¹⁶ have calculated low-energy-electron lifetimes in noble metals and ferromagnetic Co using a golden-rule-like expression for the scattering rates, simple approximations for the DOS and constant Coulomb matrix elements. First-principles calculations of the lifetime due to electron-electron interactions have been performed for image-potential states¹⁷ and for bulk states in alkali and noble metals.¹⁸ The lifetime is obtained from the inverse of the imaginary part of the self-energy. As the lifetime calculated in Fermi-liquid theory, the lifetime as calculated in the above works is a single-electron lifetime. Due to the additional effects by secondary electrons and transport in 2PPE experiments, it is difficult to compare these theoretical results with the relaxation times measured in 2PPE. For the $3d$ transition metals Fe, Co, and Ni, which show important contributions from the more localized d states in the vicinity of the Fermi energy, first-principles calculations of the lifetime of excited electrons in the range of a few eV from the Fermi energy have not to our knowledge been reported in the literature so far.

In this paper, we present both theoretical and experimental results for the electron dynamics as observed by 2PPE for Cu and ferromagnetic Fe, Co, and Ni. Systematic trends among the transition metals are discussed. A theoretical model for the 2PPE process is presented which is based on the time evolution of the distribution function. The latter is calculated with the Boltzmann equation including effects of photoexcitation, electron-electron scattering and transport of excited carriers out of the detection region. Electron-electron scattering rates are calculated from a golden-rule expression using realistic densities of states and constant Coulomb matrix elements. The approach for the calculation of the scattering rates is as outlined by Penn *et al.*¹⁵ We extend this approach to include not only the relaxation of excited electrons, but also the generation of secondary electrons. Rather than performing a first-principles calculation of the lifetime of single excited electrons, we lay emphasis on using a model which yields material-specific single-electron lifetimes for transition metals and enables us to calculate the relaxation time of the distribution including effects of secondary electrons and transport. This allows a direct comparison of calculated relaxation times with experimental results.

The structure of the paper is as follows. In Sec. II, we describe the model for the dynamics of excited electrons from which 2PPE is calculated. Numerical results for the relaxation of the distribution of excited electrons are presented in Sec. III. In Sec. IV, the experiments are described and their results are given. In Sec. V, experimental and theoretical results are compared and discussed. Conclusions and outlook are given in Sec. VI.

II. THEORY

The process of two-photon photoemission is illustrated in Fig. 1. The two-photon photoemission intensity is calculated from the non-equilibrium electronic distribution function in the intermediate state. The intensity $I^{2\text{PPE}}$ is obtained by multiplying the distribution function in the intermediate state $f(E, \sigma, z, t)$ with a factor e^{-z/λ_σ} for transmission into the vacuum¹⁹ and with the power of the laser pulse $P(t)$ and integrating over time t and coordinate z perpendicular to the surface:

$$I^{2\text{PPE}}(E + h\nu, \sigma) = \int_{-\infty}^{\infty} dt P(t) \int_0^{\infty} dz e^{-z/\lambda_\sigma} f(E, \sigma, z, t). \quad (1)$$

Energy and spin of the intermediate state are denoted by E and σ . The photon frequency is given by ν . For the transmission factor, we use the spin-averaged values of the attenuation length λ measured in overlayer experiments for different elements.²⁰ The above expression for the photoemission intensity based on the distribution function is suited for the description of the population dynamics. Our aim here is to describe incoherent electronic processes like the decay of excited electrons and the generation of secondary electrons due to electron-electron scattering. Also, the experiments with which we wish to compare our calculations are phase-averaged measurements of the decay of the population of excited electrons. The expression is further justified by the fact that for bulk states in metals, one expects rapid loss of coherence within a few fs. However, clearly, if one is mainly interested in coherent effects like the decay of the optically induced polarization, the treatment of the dynamics and the photoemission process should be based on both occupation function and polarization.^{2,21,22} Recent interferometric measurements have shown relatively long decoherence times in Cu of $T_2^\omega = 5 - 10$ fs for holes at the top of the d bands and electrons at about $E - E_F = 1$ eV and up to $T_2^{2\omega} = 35$ fs for electrons at about $E - E_F = 4$ eV.²³

As shown in Fig. 1, 2PPE involves three electronic states, in which different physical processes like electron-electron scattering, electronic transport and electron emission into the vacuum take place and determine the observed photoemission signal. First, the initial state at energy E_1 is an occupied bulk state. The spectrum of optical excitation is determined by the optical transition matrix elements between the initial and intermediate states. Optical excitation takes place within the optical penetration depth of the surface. After optical excitation, the holes left behind relax and get filled via Coulomb scattering by electrons from occupied levels closer to the Fermi energy. Energy conservation requires that at the same time other electrons from below the Fermi energy are excited to unoccupied levels above the Fermi energy (secondary electrons). The Boltzmann equation takes this process (the so-called Auger process) into account. The holes are also filled via transport processes (ballistic or diffusive) by electrons from the bulk. Secondly, the intermediate state at energy E_2 is an unoccupied bulk state between the Fermi energy and the vacuum energy. Excited electrons undergo electron-electron collisions with cold electrons in the Fermi sea. Thus, the optically excited (primary) electrons are scattered out of the intermediate state. However, also secondary electrons are scattered into the intermediate state, which leads to the refilling of this state. The intermediate, normally unoccupied state can be refilled by: i) an optically excited (hot) electron after an electron-electron scattering process; ii) a cold electron from below the Fermi energy after scattering with a hot electron; iii) an Auger process (an electron from below the Fermi energy after a hole is filled by a cold electron). The latter process leads to a dependence of the observed lifetime on the rate of filling of holes (the hole lifetime). Also, excited electrons created in the intermediate state within a penetration depth of the surface are transported into the bulk. The transport of electrons leads to the removal of electrons from the intermediate state. Note, the 2PPE technique does not distinguish between the removal by transport and the removal by electron-electron scattering to lower energy. Thirdly, the final state at energy E_3 is above the vacuum energy and describes a free electron which can escape from the solid. Its wave function decays exponentially into the solid, the decay factor being given by the mean free path of electrons above the vacuum energy. Only electrons within a mean free path of the surface absorbing a second photon are emitted into the vacuum.

We use now the Boltzmann equation taking into account the above processes to describe the time evolution of the electronic distribution function for states close to the surface of a solid. The states are characterized by energy E , spin σ , band index $\alpha = sp, d$ and coordinate z perpendicular to the surface. The Boltzmann equation reads

$$\frac{\partial f(E\alpha\sigma z)}{\partial t} = \left. \frac{\partial f(E\alpha\sigma z)}{\partial t} \right|_{\text{optical}} + \left. \frac{\partial f(E\alpha\sigma z)}{\partial t} \right|_{e-e}^{\text{in}} + \left. \frac{\partial f(E\alpha\sigma z)}{\partial t} \right|_{e-e}^{\text{out}} + \left. \frac{\partial f(E\alpha\sigma z)}{\partial t} \right|_{\text{trans}}^{\text{trans}}. \quad (2)$$

The Boltzmann equation contains the rates of change of the occupation due to optical excitation, electron-electron scattering and electronic transport perpendicular to the surface. Note, the relaxation time τ of the intermediate state which is compared with the experimental relaxation time is determined from the decay of the occupation.

To determine the relaxation time, we take the time of the maximum in the occupation. We then use the relation between the time of the maximum and the relaxation time which is known in the case of an exponential decay. The extraction of a relaxation time from the decay of the distribution by comparison with an exponential decay is equivalent to the method used in the experiments, described in Sec. IV C.

For the ferromagnetic metals, we calculate the relaxation time for excited spin-up and spin-down electrons, τ_\uparrow and τ_\downarrow . Spin-up and spin-down electrons will be denoted as majority and minority electrons in the following. The spin-averaged relaxation time τ is defined as $1/\tau = 1/2 (1/\tau_\uparrow + 1/\tau_\downarrow)$ and the relaxation time ratio as $R = \tau_\uparrow/\tau_\downarrow$.

The optical transition rate between two electronic states due to the interaction with the laser field with photon energy $h\nu$ is given by

$$\left. \frac{\partial f(E\alpha\sigma)}{\partial t} \right|_{E',\beta}^{\text{optical}} = - \sum_{E',\beta} |p(E\alpha, E'\beta, \nu)|^2 f(E\alpha\sigma) [1 - f(E'\beta\sigma)] \rho(E'\beta\sigma) \delta(E - E' - h\nu). \quad (3)$$

Here, $p(E\alpha, E'\beta, \nu)$ is an average over electron momenta of the optical transition matrix elements describing the transition between an initial occupied state in band α at energy E and a final unoccupied state in band β at energy E' . The DOS in the final state is denoted by $\rho(E'\beta\sigma)$. We use energy-independent optical transition matrix elements. Thus, the strength of the optical excitation to a specific final state energy above the Fermi energy is proportional to the initial and final density of states. Optical excitation takes place within the optical penetration depth of the surface. We assume weak optical excitations, since the energy deposited in the system is not enough to significantly disturb the temperature or magnetization. The fraction of excited electrons per atom is about 10^{-6} (see Sec. IV).

The transition rates due to electron-electron scattering are calculated using Fermi's golden rule in the random- \mathbf{k} approximation, since the strong electron-electron interaction in noble and transition metals leads to a fast redistribution of electronic momenta so that the information about the initial optical excitation process in \mathbf{k} space is quickly lost. This then justifies the random- \mathbf{k} approximation for the calculation of electronic dynamics. We extend the treatment by Penn *et al.*¹⁵ to a non-equilibrium situation by calculating scattering rates into and out of a level and taking into account the non-equilibrium distribution of electrons. The scattering rates are given in the appendix. The expressions for the transition rates for scattering out of or into a state with energy E and spin $\sigma = \uparrow, \downarrow$ are given by:

$$\frac{\partial f_{E\sigma}}{\partial t} \bigg|_{e-e}^{\text{out}} = -f_{E\sigma} \frac{1}{2} \int_{-\infty}^{\infty} dE' \left\{ h_{E'\sigma} W(E\sigma, E'\sigma) + h_{E'\bar{\sigma}} W(E\sigma, E'\bar{\sigma}) \right\} \quad (4)$$

and

$$\frac{\partial f_{E\sigma}}{\partial t} \bigg|_{e-e}^{\text{in}} = (1 - f_{E\sigma}) \frac{1}{2} \int_{-\infty}^{\infty} dE' \left\{ e_{E'\sigma} W(E'\sigma, E\sigma) + e_{E'\bar{\sigma}} W(E'\bar{\sigma}, E\sigma) \right\}, \quad (5)$$

with

$$W(E\sigma, E'\sigma) = \frac{2\pi}{\hbar} \int_{-\infty}^{\infty} d\varepsilon \left(e_{\varepsilon\sigma} h_{\varepsilon+\omega, \sigma} 2 |M^{\uparrow\uparrow}|^2 + e_{\varepsilon\bar{\sigma}} h_{\varepsilon+\omega, \bar{\sigma}} |M^{\uparrow\downarrow}|^2 \right) \quad (6)$$

and

$$W(E\sigma, E'\bar{\sigma}) = \frac{2\pi}{\hbar} \int_{-\infty}^{\infty} d\varepsilon e_{\varepsilon\bar{\sigma}} h_{\varepsilon+\omega, \sigma} |M^{\uparrow\downarrow}|^2. \quad (7)$$

Here, $e_{E\sigma} = \rho_{E\sigma} f_{E\sigma}$ is the number of electrons and $h_{E\sigma} = \rho_{E\sigma} (1 - f_{E\sigma})$ is the number of holes at energy E , with spin σ . The energies involved in the transition are E, E', ε and $\varepsilon + \omega$, where $\omega = E - E'$ is the energy transferred in the transition. The spin is denoted by σ and its opposite by $\bar{\sigma}$. For details see the appendix.

To include transport effects, we use a spatially dependent distribution function. Due to the fact that the laser spot is much larger than the optical penetration depth, we neglect transport in the direction parallel to the surface and keep only the coordinate z in the direction perpendicular to the surface. The distribution function $f(E, z)$ describes the occupation of an electronic state $|E\rangle$ at the coordinate z . Electrons in state $|E\rangle$ are moving in all directions with a certain velocity distribution. Assuming an isotropic distribution, the distribution of velocities perpendicular to the surface is constant up to a maximal velocity. The distribution of velocities v_z in z direction is described by an additional argument in the distribution function and which is now written as $f(E, z, v_z)$. Using Liouville's theorem, one can express the change in the number of electrons moving with a velocity v_z as:²⁴

$$\frac{\partial f(E, z, v_z)}{\partial t} \bigg|_{\text{trans}} = -v_z \nabla_z f(E, z, v_z). \quad (8)$$

The transport effect is based on a gradient in the particle density which is created by the photoexcitation within the optical penetration depth. We neglect the weak energy dependence of the velocity a few eV above the Fermi energy. We take into account the fact that sp and d electrons have different velocities due to their different degree of localization. The velocity of an electron in band α with wave vector k is given by $v_\alpha(k) = \frac{1}{\hbar} \frac{\partial E_\alpha(k)}{\partial k}$. Thus, nearly free electrons in sp -like bands have higher velocities (or smaller effective mass) than more localized electrons in flat, d -like bands. For s electrons, we take the Fermi velocity as the maximal velocity. For d electrons, we note that the velocity is roughly proportional to the band width and we therefore set $v_d/v_s = W_d/W_s$. For all elements considered, we use $v_F = 18 \text{ \AA/fs}$ and $W_d/W_s = 0.4$.^{25,26} Thus, we distinguish between different elements purely by the relative contribution of sp and d electrons. We also take into account the effect of inelastic electron-electron scattering on transport. At each time step we determine the fraction of electrons at energy E which undergo inelastic scattering from Eqs. (4–5) and randomly redistribute their velocities.

The physical content of the electron-electron scattering rates in Eqs. (4–5) is that the transition rates are determined by the available phase space for a transition weighted by the square of the transition matrix element. The scattering rates presented above also describe the formation of the secondary-electron cascade. Scattering out of an excited level, due to relaxation, and scattering into an excited level, due to excitations, are treated on the same footing. The two processes occur simultaneously because of energy conservation. The rate $\frac{\partial f(E\sigma)}{\partial t}\bigg|_{e-e}^{\text{in}}$ for scattering into a level contains the effects leading to the refilling of the intermediate state. By calculating the scattering rates in a consistent manner for states above and below the Fermi energy, we keep track of the creation and relaxation of electrons as well as holes. In this way, the refilling of levels above the Fermi energy by secondary electron generation is included in the calculation.

Note, from the Boltzmann equation we recover the Fermi-liquid behavior $\tau(E) \propto (E - E_F)^{-2}$ in the limiting case of a single excited electron with energy close to the Fermi energy. To see this we consider only the term $\frac{\partial f(E\sigma)}{\partial t}\bigg|_{e-e}^{\text{out}}$ describing the relaxation by electron-electron scattering. Since we consider a single excited electron at energy E , the scattering rate $\frac{\partial f(E\sigma)}{\partial t}\bigg|_{e-e}^{\text{in}}$ into the level is zero. We assume that the optical excitation has stopped and neglect the transport term. If we take the equilibrium distribution function for $f(E\sigma)$, the integrals become time-independent and the remaining term in the Boltzmann equation can be written as $\frac{\partial f(E\sigma)}{\partial t}\bigg|_{e-e}^{\text{out}} = -\frac{f(E\sigma)}{\tau(E\sigma)}$ with the definition $1/\tau(E\sigma) = 1/2 \int_{-\infty}^{\infty} dE' \{h_{E'\sigma} W(E\sigma, E'\sigma) + h_{E'\bar{\sigma}} W(E\sigma, E'\bar{\sigma})\}$ for the inverse lifetime. For simplicity now we neglect spin-dependent effects and take $\rho = \rho_{\uparrow} = \rho_{\downarrow}$ and $M^{\uparrow\uparrow} = M^{\uparrow\downarrow} = M$. Then the equilibrium distribution function limits the range of the integrations and the inverse lifetime reduces to

$$\frac{1}{\tau(E)} = \frac{2\pi}{\hbar} \int_0^E dE' \rho(E') \int_{-\omega}^0 d\varepsilon 2\rho(\varepsilon) \rho(\varepsilon + \omega) |M|^2 ,$$

where $\omega = E - E'$. One sees the influence of the density of states within the distance $(E - E_F)$ of the Fermi energy and of the Coulomb matrix element. For energies very close to E_F or for constant DOS ρ one obtains

$$\frac{1}{\tau(E)} = \frac{2\pi}{\hbar} \rho^3 |M|^2 (E - E_F)^2 . \quad (9)$$

Note, due to energy conservation in electron-electron scattering the inverse lifetime is proportional to ρ^3 . In addition to the factor ρ from the relaxation of the initial electron at energy E , one also has to take into account the available phase space for the electron-hole pair created because of energy conservation, which yields a factor of ρ^2 . This may be compared with the Fermi-liquid-theory expression for the electronic lifetime which is given by^{27,28}

$$\tau(E) = a_0(r_s)(E - E_F)^{-2} , \quad (10)$$

where $a_0(r_s) = 263r_s^{-5/2}$ fs eV² and r_s is the dimensionless parameter describing the density of the electron gas. It is given by the relation $1/n_e = 4\pi(r_s a_0)^3/3$, where n_e is the electron density and a_0 is the Bohr radius. Thus, the expression for $\tau(E)$ derived from $\frac{\partial f(E\sigma)}{\partial t}\bigg|_{e-e}^{\text{out}}$ in the appropriate limit gives the same energy dependence as Fermi-liquid theory.

One can try to understand the lifetimes observed in different metals by means of the Fermi-liquid-theory expression for τ by using r_s corresponding to the electron density in the metal. However, the expression is strictly valid only for free-electron-like metals and it is not simple to extend it to take into account d electrons. First one can use the electron density corresponding to sp electrons only. We take values for integrated sp and d electron densities of states in the solid from Ref. 29. The number of sp electrons per atom for Fe, Co, Ni, and Cu is 1.07, 1.13, 1.03 and 1.10, respectively. One obtains roughly $r_s \sim 2.6$ and $a_0 \sim 25$ fs eV² for all the metals Fe, Co, Ni, and Cu. This neglects d electrons altogether and does not yield any differences between these metals. On the other hand, if one uses the total number of sp and d electrons, one obtains values for r_s monotonically decreasing from $r_s = 1.32$ in Fe to $r_s = 1.22$ in Cu, leading to $a_0 = 130$ fs eV² for Fe and $a_0 = 161$ fs eV² for Cu. It is evident from the magnitude of a_0 that this overestimates the influence of d electrons. Clearly a more refined treatment is necessary which distinguishes between sp and d electrons and takes into account the DOS within a few eV of the Fermi energy. The influence of the d bands on the lifetime of a state depends on the distance E_d of the d bands to the Fermi energy: for small excitation energy $\Delta E = E - E_F < E_d$, the d bands should have little influence on the lifetime. In Sec. V, we will discuss the influence of d bands in more detail.

III. NUMERICAL RESULTS OF THE THEORY

We discuss the results for the calculated relaxation time in Cu and in the transition metals Fe, Co, and Ni taking into account different physical effects determining the relaxation time. To show clearly the influence of different physical mechanisms, the calculated relaxation times are presented in three steps including consecutively more processes in the calculation: single-electron lifetime, relaxation time of the distribution including secondary electrons, and relaxation time of the distribution including secondary electrons and transport.

In the first step, we consider the single-electron lifetime. At this level, we take into account in the Boltzmann equation, Eq. (2), only scattering out of a particular level. Hence, only the term $\frac{\partial f(E\alpha\sigma)}{\partial t}\bigg|_{e-e}^{\text{out}}$ is kept. Results are labelled by (*out*) in Figs. 3 and 5. After photoexcitation, the time evolution of the distribution function shows an exponential decay. The lifetime obtained in this way is a single-electron lifetime, since it contains only information about a single electronic level under consideration. This single-electron lifetime can be compared with the lifetime calculated in Fermi-liquid theory or obtained from first-principles calculations of the self-energy.¹⁸ It does not contain effects of the distribution (like the refilling of intermediate levels) and it is independent of the photon energy, laser intensity etc. However, the single-electron lifetime is observed in an experiment only if there are no other effects present such as secondary-electron generation or transport. Thus, the calculated single-electron lifetime should not be directly compared with experimental results. It serves as a guide for comparison with other theoretical results for the single-electron lifetime and as a reference for comparison with results for the relaxation time when secondary electrons and transport are included.

In the second step, we take into account secondary electrons also, while neglecting transport effects. Thus, in the Boltzmann equation, we keep the electron-electron scattering terms for scattering *into* and *out of* the levels. Results are labelled (*out, in*). The in- and out-scattering rates are calculated on the same footing from the golden-rule expressions for the transition rate given in Eqs. (4–7). They are determined by the densities of states, non-equilibrium distribution function and Coulomb matrix elements. The relaxation time obtained in this approximation is not only a function of the level under consideration, but it includes effects of the whole distribution. Note, it is not a single-electron lifetime, but an effective relaxation time of the distribution.

In the third step, we also take into account transport effects. In addition to the electron-electron interaction, the loss of excited electrons due to transport out of the surface region will influence the occupation and hence the apparent electronic relaxation time. Results are labelled (*out, in, transport*).

The DOS for the different metals used as input in the calculation of the scattering rates in Eqs. (4–7) are taken from an FLAPW calculation³⁰ and are shown in Fig. 2. We distinguish only between *d*-like and *sp*-like states in the DOS. We take the partial *d* DOS from the calculation and use the remaining DOS as *sp*-like DOS. Thus, our partial DOS for *sp*-like states includes all contributions apart from the *d* states. The total DOS are very similar to the ones given in Ref. 25. For Cu, however, we shift the *d* bands to lower binding energy by 0.4 eV in order to obtain agreement with ARPES results for the binding energy of the *d* bands.¹⁹ It is known that LAPW calculations might yield too small binding energies for the *d* bands.³¹

The values for the optical penetration depth for the calculation were obtained using the optical constants given in Ref. 32 and are shown in Table I.

A. Numerical Results for Cu

Fig. 3 illustrates the effect of secondary electrons and transport on 2PPE intensity and relaxation time for optical excitation with photon energy $h\nu = 3.3$ eV. For the calculation we use for the Coulomb matrix elements $M = 0.8$ eV and $|M^{\uparrow\uparrow}/M^{\uparrow\downarrow}| = 1$. This choice will be justified at the end of this section. The results for Cu show particularly clearly the influence of secondary electrons and transport.

In curve *a* of Fig. 3, we show the 2PPE intensity calculated from Eq. (1) without including scattering or transport terms in the Boltzmann equation. In this case the 2PPE intensity is proportional to the number of optically excited electrons in the intermediate state. The optical excitation in Eq. (3) is proportional to the convolution of initial and final DOS, since we use constant optical transition matrix elements. The intensity shows an important contribution from initial states in the *d* band below $E - E_F = 1.6$ eV with a pronounced peak at 1.4 eV and a small contribution from initial states in the *s* band above 1.6 eV.

In curve *b* of Fig. 3, we show the calculated 2PPE intensity keeping only the out-scattering term in Eq. (2), which corresponds to an exponential decay of the optically excited distribution. The intensity is reduced compared to the intensity without scattering, and the reduction gets stronger towards higher excitation energy due to the shorter lifetime. The relaxation time calculated in this way is a single-electron lifetime. For energies below $E - E_F = 2$ eV,

the single-electron lifetime shows the energy dependence $\tau(E) \propto (E - E_F)^{-2}$ as in Fermi-liquid theory. The lifetime resulting from Fermi-liquid theory for Cu with $a_0 = 25$ fs eV² is shown by curve *e*. It is a factor of about 2.5 lower than the lifetime calculated using $M = 0.8$ eV.

In curve *c* of Fig. 3, we show the results using the in-scattering term as well as the out-scattering term in Eq. (2). The in-scattering term describes the generation of secondary electrons. At low energy a secondary-electron tail forms in the 2PPE intensity and the intensity becomes a superposition of the initial optical excitation and the secondary-electron tail. The relaxation time shown by curve *c* is an effective relaxation time of the distribution including secondary-electron effects. It is no longer monotonous and shows a distinct feature in the region of the peak in the intensity. We find a relative minimum in the relaxation time at the position of the peak in the intensity. Further, the relative maximum in the relaxation time corresponds to the *d*-band threshold above which very few optically excited *d* electrons are found. We can understand the feature in the relaxation time by studying the contribution of secondary electrons to the intensity. Comparing the intensity without secondary electrons (curve *b*) with the one including secondary electrons (curve *c*), we find that in the region of the peak the intensity with secondary electrons is only slightly increased compared to the intensity without secondary electrons, whereas it is strongly increased in the region above the *d*-band threshold. This shows that in the region of the peak one observes mainly relaxation of optically excited electrons, whereas above the *d*-band threshold, one finds mainly contributions of secondary electrons. Comparing the relaxation times with and without secondary electrons, we find that in the region of the peak and also at high energies $E - E_F > 2.5$ eV, the relaxation time with secondary electrons (curve *c*) comes very close to the relaxation time without secondary electrons (curve *b*), again showing that one observes mainly relaxation in these regions. Most secondary electrons are generated in the process of filling the holes in the *d* band created by the optical excitation (so-called Auger effect). The increase in the relaxation time is due to the fact that secondary electrons are generated with a certain delay after the optical excitation corresponding to the *d*-hole lifetime.^{9,33}

In Fig. 3 curve *d* shows the results obtained using transport in addition to secondary-electron effects. Compared to the case without transport (curve *c*), the 2PPE intensity is reduced. The transport effect removes excited particles from the observation region close to the surface into the bulk and thus reduces the 2PPE intensity. The relaxation time including transport (curve *d*) has a similar shape as the relaxation time with secondary-electron effects (curve *c*), but the magnitude of the relaxation time is strongly reduced by transport. Interestingly, the relaxation time including secondary electrons and transport comes close to the single-electron lifetime (curve *b*) in the region above the peak ($E - E_F > 1.6$ eV). Thus, we find that for Cu in a certain energy range, the effects of secondary electrons and transport on the observed relaxation time roughly cancel each other. This fact has been pointed out in an analysis of a 2PPE experiment before.³⁴ The effect is somewhat accidental, since it depends on the relative values of the single-electron lifetime and the transport parameters in Cu. For example, a smaller transport velocity would lead to a weaker reduction of the relaxation time under the influence of transport.

Fig. 4 shows theoretical and experimental results for the 2PPE intensity and relaxation time for photon energies $h\nu = 3.0$ and 3.3 eV. Both the peak in the intensity and the feature in the relaxation time shift linearly with photon energy. As indicated by the dotted lines, the minimum in the relaxation time corresponds to the peak in the intensity, whereas the maximum in the relaxation time corresponds to the *d*-band threshold.

For the calculations we have used a Coulomb matrix element $M = 0.8$ eV. With this choice we obtain at $E - E_F = 1$ eV for the single-electron lifetime $\tau = 55$ fs and for the relaxation time including secondary electron and transport effects $\tau = 40$ fs (for photon energy $h\nu = 3.3$ eV). This is in good agreement with first-principles calculations for the single-electron lifetime¹⁸ in the energy range $E - E_F < 2$ eV. It also yields good agreement with experimentally determined relaxation times at low energies ($E - E_F \approx 1$ eV).⁹ We remark that at higher energies ($E - E_F > 2$ eV), we would obtain better agreement with first-principles calculations and experiments for a smaller Coulomb matrix element $M = 0.6$ eV. Thus, the use of energy-dependent matrix elements might improve the overall agreement between theory and experiment over a wide energy range.

B. Numerical Results for Fe, Co, and Ni

First, we discuss numerical results shown in Figs. 5a and b and labelled by (*out*) for the single-electron lifetime in Fe, Co, and Ni. They are obtained by including only the relaxation term $\frac{\partial f(E\alpha\sigma)}{\partial t}\bigg|_{e-e}^{\text{out}}$ for scattering out of a level. We use the same energy-independent Coulomb matrix element $M = 0.8$ eV and $|M^{\uparrow\uparrow}/M^{\uparrow\downarrow}| = 1$ for the different metals.

For constant and equal Coulomb matrix element M , the single-electron lifetime can be directly related to the DOS shown in Fig. 2 and used as input for the calculation. The influence of the DOS on the single-electron lifetime is seen in the scattering-rate expression Eq. (4) or in the simplified expression Eq. (9). The scattering rate, the inverse of the lifetime, is proportional to a combination of terms which are all products of three factors of the DOS. The first factor

represents the free states available for the relaxation of the initial electron, the second factor represents the occupied states containing possible scattering partners for the electron-electron collision, and the third factor stands for the unoccupied state into which the second electron is scattered during the transition.

When comparing the single-electron lifetime of Cu shown in Fig. 3 (curve *b*) with the results in Fig. 5a for the transition metals, one can see that Cu has a lifetime much longer than the other metals. This is due to the small total DOS close to the Fermi energy. In Cu, the *d* bands are located about 2 eV below the Fermi energy and there is only a very small total DOS close to the Fermi energy (Fig. 2). The small *d* DOS close to the Fermi energy is due to hybridization with *sp*-like states. In Ni with one electron less than Cu, the *d* bands move closer to the Fermi energy. Furthermore, the *d* bands are split into a minority and majority spin band and a small portion of the minority *d* band is unoccupied, extending up to about 0.4 eV above the Fermi energy (Fig. 2). Due to the pronounced peak at the upper edge of the *d*-band DOS, the minority DOS close to the Fermi energy is extremely large. This leads to a large phase space for electron-electron scattering at low energy. Thus at low energy (below $E - E_F = 1$ eV), Ni has the smallest calculated single-electron lifetime among the four elements. Co, with one electron less than Ni, has an even larger portion of unoccupied minority DOS, extending up to about 1.2 eV above the Fermi energy. Although the total number of unoccupied states is higher in Co than in Ni, the minority DOS at the Fermi energy is lower in Co. Thus at low energy (below 1 eV), Co has less phase space for electron-electron scattering and the calculated lifetime is longer than in Ni. With increasing energy, more and more unoccupied states become available in Co, so that above 1 eV, the calculated single-electron lifetime in Co becomes shorter than the one in Ni. In Fe, again with one electron less compared to Co, the unoccupied minority DOS extends up to 2.4 eV above the Fermi energy, and even the majority DOS has a small unoccupied fraction. The minority DOS at the Fermi energy in Fe is lower than in Co and in Ni, so that Fe has the smallest phase space and the longest calculated lifetime at low energy.

Therefore, at low energy (below $E - E_F = 1$ eV), our simplified theory with equal M for the different metals gives $\tau_{Ni} < \tau_{Co} < \tau_{Fe}$. This trend changes for Co and Ni above 1 eV. Then we get $\tau_{Co} < \tau_{Ni}$. At even higher energy (above 2 eV, not shown in the figure), all of the unoccupied *d* states in Fe are available for a transition and one calculates $\tau_{Fe} < \tau_{Co} < \tau_{Ni}$. This relation is also observed in transmission experiments above the vacuum energy for electrons with energies above $E - E_F = 5$ eV.³⁵

In Fig. 5b the ratio of majority to minority single-electron lifetime $\tau_{\uparrow}/\tau_{\downarrow}$ is shown. For Co, the lifetime ratio is nearly constant with a value $\tau_{\uparrow}/\tau_{\downarrow} = 7.5$. This is understandable in view of the high and nearly constant ratio of minority to majority DOS at low energy. For Ni the lifetime ratio decreases from $\tau_{\uparrow}/\tau_{\downarrow} = 9.5$ at $E - E_F = 0.4$ eV to $\tau_{\uparrow}/\tau_{\downarrow} = 4$ at $E - E_F = 1.4$ eV. The decrease of the lifetime ratio is due to the fact that above 0.4 eV there are no more unoccupied minority *d* states. The additional phase space gained by going to higher energy is the same for minority and majority electrons, leading to a smaller ratio. In Fe the ratio increases from $\tau_{\uparrow}/\tau_{\downarrow} = 0.5$ to 1 for excitation energies between $E - E_F = 0.4$ and 1.2 eV. Thus, majority electrons have a shorter calculated lifetime than minority electrons at low energy. This results from the unoccupied portion of the majority DOS above the Fermi energy, which for low energy leads to a larger phase space for the relaxation of majority electrons and therefore to a shorter lifetime.

Secondly, we discuss results shown in Figs. 5c and d obtained when secondary electrons are included in the calculation. They are labelled by (*out*, *in*). Transport effects are still neglected. In the Boltzmann equation, Eq. (2), we now keep the terms $\frac{\partial f(E\alpha\sigma)}{\partial t}\bigg|_{e-e}^{\text{out}}$ and $\frac{\partial f(E\alpha\sigma)}{\partial t}\bigg|_{e-e}^{\text{in}}$, while neglecting $\frac{\partial f(E\alpha\sigma)}{\partial t}\bigg|_{e-e}^{\text{trans}}$. In contrast to the single-electron lifetime, the relaxation time calculated including secondary electrons is an effective relaxation time of the distribution. The inclusion of secondary electrons leads to an increase of the relaxation time by a factor of about 2 time as compared to the single-electron lifetime. The strongest effect is found at the lowest energies. The increase in the relaxation time is stronger for the elements with the shortest calculated lifetimes (Ni, Co), so that the differences in the relaxation time including secondary electrons between Ni, Co, and Fe are smaller than for the single-electron lifetime. The ratio $\tau_{\uparrow}/\tau_{\downarrow}$ for Ni and Co is reduced to $\tau_{\uparrow}/\tau_{\downarrow} = 4 - 5$ for Ni and $\tau_{\uparrow}/\tau_{\downarrow} = 5 - 6$ for Co. For Fe, the ratio is nearly unchanged, $\tau_{\uparrow}/\tau_{\downarrow} = 0.5 - 1$. The reduction of the ratio $\tau_{\uparrow}/\tau_{\downarrow}$ due to secondary electrons is understandable in view of the fact that the inclusion of secondary electrons leads to a coupling between majority and minority electron populations via electron-electron scattering. Relaxing minority electrons can excite majority electrons and vice versa. For Co and Ni, for example, longer-living majority electrons will continue to excite minority electrons after the shorter-living primary minority electrons have relaxed. The apparent minority-electron relaxation time becomes longer and the ratio $\tau_{\uparrow}/\tau_{\downarrow}$ becomes smaller by this process. The trends among the calculated relaxation times of the transition metals, particularly the relation $\tau_{Ni} < \tau_{Co} < \tau_{Fe}$ at $E - E_F < 1$ eV are unchanged when secondary electrons are included.

The spectral shape of the optical excitation, i.e. the distribution of primary electrons, has some influence on the calculated relaxation time. For example, electrons excited to a high energy lead to more secondary electrons (due to the short lifetime of the primary electrons) and to a distribution extending to higher energy (due to the high energy of the primary electrons). Similar arguments apply to the energetic position of the holes created by the optical excitation. The results for the transition metals shown in Fig. 5 are obtained using an optical excitation with photon

energy $h\nu = 3.0$ eV and constant optical transition matrix elements in Eq. (3). We have also studied the effect of a different optical excitation on the relaxation time. We have modelled a resonant optical excitation where excitations take place dominantly between an initial state at the top of the d band and a final state in the sp band. No significant difference in the calculated relaxation time for the two different shapes of the excitation is obtained.

Thirdly, we discuss results of the calculations including transport in addition to secondary-electron effects in the Boltzmann equation, Eq. (2). They are labelled by (*out*, *in*, *transport*). Results are shown in Figs. 5e and f. The inclusion of transport leads only to a very slight reduction of the effective relaxation time in Fe, Co, and Ni. This is in contrast to the strong reduction of the effective relaxation time in Cu (compare curves *c* and *d* in Fig. 3). This is easy to understand, since the typical transport relaxation timescale in Cu is about 40 fs.^{4,9} This is shorter than, or comparable to, the single-electron lifetime in Cu in the energy range considered, but considerably longer than the typical lifetimes in Fe, Co, or Ni. Thus, transport is expected to have great influence for Cu, but not for the transition metals. The calculation yields this behavior. The ratio $\tau_{\uparrow}/\tau_{\downarrow}$ as well is only slightly affected by transport.

IV. EXPERIMENT

A. TR-2PPE technique

The TR-2PPE pump-probe experiments are carried out in a UHV chamber by monitoring the number of electrons at a given kinetic energy as a function of the delay between the pump and probe pulses. We employ the equal-pulse correlation technique, i.e. the two pulses are monochromatic and equal in intensity, but cross-polarized. For metals, the use of orthogonal linear polarized light pulses suppresses coherent interference effects (within the limit of rapid dephasing) to a large extent.⁴ Otherwise they influence the optical transition process and would make the reconvolution of the raw data much more difficult. Furthermore, the influence of Cs-induced surface states on the lifetime can be suppressed (see below).

The non-linearity of the two-photon process leads to an increase in the 2PPE yield when the pulses are spatially and temporarily superimposed. As long as the two laser pulses temporarily overlap it is obvious that an electron can be emitted by absorbing just one photon from each pulse. However, if the pulses are temporarily separated, then an excited electron from the first pulse is able to absorb a photon from the second pulse but only as long as the inelastic lifetime of the intermediate state exceeds the delay or the normally unoccupied electronic state is refilled by a secondary electron. Due to a precise measurement of the time delay between the two pulses (1 fs $\hat{=}$ path length difference of 0.3 μm), this technique allows us to analyze relaxation times which are considerably shorter than the laser pulse duration.

We use laser pulses at low fluence and peak power to avoid space-charge effects or highly excited electron distributions. We emphasize that the count rate is much lower than one electron per pulse. Therefore, we measure the relaxation and transport of individual excited electronic states rather than the collective behavior of transiently heated non-equilibrium distribution. We have to roughly calculate the fraction of excited electrons. Typically, we have a laser fluence of about 0.3 nJ/pulse in each beam resulting in 6×10^8 photons per pulse. For a spot size of $\sim 150 \mu\text{m}$ and a penetration depth of the blue light of $\sim 150 \text{ \AA}$, the volume in which the laser light will be absorbed is about $3 \times 10^{-10} \text{ cm}^3$. If 10% of the light is absorbed by the metal, then 6×10^7 photons are absorbed by 7×10^{13} atoms which results in a fractional excitation of roughly 1 part in 10^6 .

B. Experimental set-up

A schematic overview of the experimental set-up is shown in Fig. 6. The samples are mounted in a UHV chamber with a base pressure in the 10^{-11} mbar range. It is equipped with a cylindrical sector electron energy analyzer (CSA) and a spin analyzer, based on spin-polarized low-energy electron diffraction (SPLEED).³⁶ The earth's magnetic field is shielded by μ -metal coverings inside the chamber. Standard surface-physics methods such as Auger-electron spectroscopy (AES) and low-energy electron diffraction (LEED) are available to check the cleanliness and the surface structure of the samples. The orientation of the samples is 45° with respect to the laser beam and the electrons are detected in normal-emission geometry. Remanent magnetization of the ferromagnetic samples is achieved by a magnetic field pulse from a coil. The geometric arrangement of the spin analyzer allows the measurement of the spin polarization along the horizontal in-plane axis of the sample. To minimize the effects of stray fields and to facilitate electron collection, a bias voltage (-4 V for Cu and -15 V for Ni, Co, and Fe) is applied between the sample and the CSA. For spin-resolved measurements the electrons are guided into the SPLEED analyzer, which is located on top of the CSA. In this spin analyzer the electrons are first accelerated to 104.5 eV kinetic energy, as the highest figure of

merit for this kind of analyzer is known to be at this primary-electron energy.³⁶ Thereafter, the electrons are scattered at a tungsten (001) crystal. From the resulting LEED feature, the (-2,0) and (2,0) electron beams that have a high spin asymmetry, are counted in two different channeltrons. The Sherman factor S , a quantity for the spin selectivity of an analyzer, is found to increase from 0.2 to 0.25 over the two years of operation; the highest value was reached after having the tungsten SPLEED crystal a long period in very low pressure.

The time-resolved 2PPE experiments are performed with a femtosecond mode-locked Ti:sapphire laser, pumped by about 10 W from a cw Ar⁺ laser. The system delivers transform-limited and sech² temporal shaped pulses of up to 9 nJ/pulse with a duration of 40 fs at a repetition rate of 82 MHz. The linearly polarized output of the Ti:Sapphire laser is frequency-doubled in a 0.2 mm thick Beta Barium Borate (BBO) crystal to produce UV pulses at $h\nu = 3$ to 3.4 eV. The UV beam is sent through a pair of prisms to pre-compensate for pulse broadening due to dispersive elements like lenses, beamsplitters and the UHV-chamber window in the optical path. A GVD and intensity-loss matched interferometric autocorrelator set-up is used for the pump-probe experiment (see Fig. 6). The pulses are split by a beamsplitter to equal intensity (pump and probe pulses), and one path is delayed with respect to the other by a computer-controlled delay stage. Both beams are combined co-linearly but cross-polarized by a second beamsplitter and are focused at the sample surface.

For the ferromagnetic samples, we use evaporated films because they can be held magnetized in a single-domain state without an applied external field and the stray field is much smaller compared to a bulk ferromagnet. In principle, this experiment could also be performed with bulk samples. The ferromagnetic films are evaporated onto a Cu(001) substrate in a separable chamber. We use a water-cooled evaporator based on electron-beam heating. The material to be evaporated (of 99.999% purity) was inside a molybdenum crucible (Co, Fe) or directly evaporated from a 1 mm thick wire (Ni). The evaporation rate (around 0.2 nm/min) was checked with a quartz oscillator, which is calibrated against atomic-force-microscope thickness measurements. During evaporation the pressure remained in the 10⁻¹⁰ mbar region.

The thickness of the ferromagnetic films must fulfill the following requirements. Firstly, it has to be large enough, in order to avoid an influence of electrons from the Cu substrate. Secondly, it should be possible to remanently magnetize the film by a suitable strong field pulse. And thirdly, the axis of the magnetization has to lie in the film plane because the geometry of our spin analyzer only allows the measurement of transversally polarized electrons.

Cobalt films, epitaxially grown on Cu(001) surfaces, are formed in a stable fcc structure and exhibit in-plane magnetization. For thick films, the in-plane magnetization easy axis lies along the (110) direction of the Cu crystal.³⁷ In-plane magnetization was detectable starting at a thickness of around 0.4 nm. This is in agreement with other investigations using the magneto-optical Kerr effect.³⁸ Above a film thickness of 2 nm, the spin polarization did not increase any more on further deposition of Co. For our investigations we evaporated 10 nm thick Co films.

Iron grows in the fcc structure on Cu(001) during the initial steps of evaporation. The magnetization vector is oriented perpendicular to the film surface. Above a thickness of around 2 nm a bcc (110) structure starts developing.³⁹ The magnetic easy axis for these thick films is found to lie parallel to the Cu(100) axis.⁴⁰ We use 20 nm thick iron films for our investigation.

For Ni on Cu(001) the magnetization vector is in-plane for small thicknesses, then it switches to out-of-plane at a thickness of around 1.2 nm.⁴¹ Only at larger thicknesses of around 6-7 nm does it turn back to in-plane.⁴² We found a saturation of the spin polarization for thicknesses above 25 nm. Therefore, we evaporated 40 nm thick Ni films for our measurements.

The clean metal surfaces are first dosed with Cs to lower the surface work function, a well-known technique. This enabled lifetime measurements of lower excited states, increasing the useful energy range of the spectra closer to the Fermi energy (see Fig. 1). Cs is evaporated from a thoroughly out-gassed getter source (SAES). The effect on the lifetime by dosing a metal surface with small amount of Cs (<0.1 ML) has been thoroughly investigated in the last years.^{43,44} Using cross-polarized pulses no differences in the lifetime have ever been found between a clean and a cesiated metal surface by means of TR-2PPE.⁴⁵ In addition, we found no differences in spin polarization between the clean and the cesiated surfaces in the overlapping energy region between 1.7 and 3.3 eV.

C. Experimental results for Cu

In Fig. 4b the extracted relaxation time as a function of the intermediate-state energy for a Cu(111) surface is shown, using a photon energy of 3.0 eV (□) and 3.3 eV (○). The data are deconvoluted from the experimentally obtained cross-correlation traces using a rate-equation model for the population of the intermediate state. In the case of rapid dephasing, and assuming an exponential depletion of the nascent photoexcited electron population, the evolution of the transient population $N^*(t)$ of the intermediate state is given by $dN^*(t)/dt = A(t) - N^*(t)/\tau$ where $A(t)$ is the excitation induced by the first (pump) laser pulse. The extraction of the relaxation time by comparison

with an exponential decay is also used in the calculation of the relaxation time as discussed in Sec. II. As expected, the lifetime increases as the excited state energy decreases, caused by the reduced phase space for electron-electron scattering (see Secs. II, III A, and Fermi-liquid theory). However, at an intermediate-state energy, where the intensity becomes dominated by interband transition from the d band to the unoccupied sp band (strong d -band peak in the intensity), the measured relaxation time decreases by more than a factor of two before it increases again. By changing the photon energy from $h\nu = 3.0$ eV to $h\nu = 3.3$ eV, both the d -band peak in the intensity and the dip in the measured lifetime move with the same energy difference $\Delta E = \Delta h\nu$ as expected. The striking difference in the values observed in the energy range $E - E_F = 0.7 - 1.3$ eV indicate quite clearly that the relaxation time can depend critically on the used photon energy.

D. Experimental results for Fe, Co, and Ni

1. Spin-integrated time-resolved 2PPE measurements

We used the same equal-pulse correlation technique to extend the investigation of the hot-electron relaxation to transition metals Co, Fe, and Ni. Compared with noble metals, in which the d shell is completely filled (see Cu and Ag), the d band of transition metals is only partially filled, and the electronic and relaxation properties are dominated to a considerable degree by these d electrons. The strong localization of these d electrons results in a narrower band and hence in a much higher density of states near the Fermi level as compared with the sp electrons in Cu and Ag. A higher density of occupied and unoccupied states near the Fermi level is expected to lead to faster relaxation and hence to a shorter inelastic lifetime of excited electronic states as discussed in Sec. III B. This prediction is well satisfied by our data. Fig. 7 shows a comparison of the extracted relaxation time of silver and the three investigated ferromagnetic transition metals cobalt, nickel and iron. The experimental values for these metals are at least a factor of 10 smaller than those of Cu and Ag. These small values reduce the energy range in the region of 0.3 eV to 1.3 eV which provides a meaningful statement about the relation in the relaxation time between the three investigated transition metals. In contrast to the numerical results calculated using the same Coulomb matrix element M for different metals (see Sec. III B), the data indicate a relation $\tau_{\text{Fe}} < \tau_{\text{Ni}} < \tau_{\text{Co}}$ within this energy range.

2. Spin- and time-resolved 2PPE measurements

Adding a spin analyzer to the CSA energy analyzer makes possible the separate but simultaneous measurement of both spin states. The electrons of a fixed energy are counted according to their spin in two different channeltrons as a function of the time delay between the two pulses, at a given magnetization direction. To compensate for an apparatus-induced asymmetry, the magnetization is then reversed and the measurement is taken again. From the resulting four datasets the relaxation times τ_{\uparrow} and τ_{\downarrow} for spin-up and spin-down electrons are extracted by using the same deconvolution method as discussed above. Each pair of data points presented in the plots of this section is the average of eight to ten single relaxation time measurements.

The spin dependence will have a superimposed effect on the spin-integrated relaxation time. Therefore, a spin dependence in the relaxation time can only be resolved if there is already a certain relaxation time detectable with spin-integrated measurements. As shown in Fig. 7, in the energy range above 1.4 eV, we find for all three transition metals a relaxation time smaller than our time resolution (< 2 fs). On the other hand, at intermediate-state energies close to E_F , the electrons emitted by 1PPE processes start becoming important. They induce a large background to the 2PPE signal and make an accurate extraction of the lifetimes difficult. Therefore, spin-resolved measurements can only be usefully performed for intermediate-state energies between 0.3 and 1.1 eV.

In Fig. 8 the spin-dependent relaxation time for electrons (upper part) and the ratio of majority to minority lifetime (lower part) of Fe, Co, and Ni films are plotted. The error bars in the plot represent the statistical scatter. The experimental results of the three examined ferromagnetic materials show two common facts: i) The lifetime for majority-spin electrons is always found to be longer than the lifetime for minority-spin electrons and ii) the value for $\tau_{\uparrow}/\tau_{\downarrow}$ was found to lie between 1 and 2. The largest differences between τ_{\uparrow} and τ_{\downarrow} are found for Ni and Co, whereas for Fe, the difference is slightly reduced. This qualitative behavior of the spin-dependent lifetime can be readily explained by the excess of unfilled minority-spin states compared to unfilled majority-spin states. According to this simple model, the spin dependence of the scattering rate is larger for the strong ferromagnets Co and Ni than for the weak ferromagnet Fe. This is in agreement with our measurements, where only a small spin effect could be detected for Fe. In Fe, this model would even predict a reversal of the effect for low energies below 1 eV, i.e. the lifetime for spin-down electrons should become longer than the lifetime for spin-up electrons, see Fig. 5b. A ratio of majority to minority

relaxation time R below 1 is, however, not observed for $E - E_F < 1$ eV. This result indicates that the simple model, considering the different number of empty electronic states as the only decisive factor for a spin-dependent relaxation time, is not sufficient for a quantitative interpretation of our experimental data.

V. DISCUSSION

First, in Fig. 4 we compare experimental and theoretical results for Cu for photon energies $h\nu = 3.0$ and 3.3 eV. Experimental and theoretical results show qualitative agreement regarding the main features. The peak in the intensity and the feature in the relaxation time (relative minimum and maximum) shift linearly with photon energy. The minimum in the relaxation time corresponds to the peak in the intensity and the maximum in the relaxation time corresponds to the d -band threshold. The explanation that the feature in the calculated relaxation time is due to the secondary electrons was given in detail in Sec. III A. The good agreement between calculated and experimental results is a strong evidence for this explanation. The calculations reproduce the features observed in different experiments^{7–9} in a natural way by including secondary electrons without invoking further explanations such as excitonic states involving $3d$ electrons.⁸ The differences between theoretical and experimental results in Fig. 4 lead to several conclusions. Both the peak in the intensity and the difference between the minimum and maximum of the relaxation time are more pronounced in the experiment than in the calculation. This may be an evidence that the calculation yields too many secondary electrons which cause a too strong background and thus a too small structure in the 2PPE intensity (see the upper part of Fig. 4a). The relatively small increase from the minimum to the maximum in the calculated relaxation time should not be affected much by this, but may rather point to the fact that the lifetime of the d holes in the calculation is too small. Note, due to the large d DOS below E_F , there is no symmetry between hole lifetimes and lifetimes of excited electrons. In our calculations, hole lifetimes for energies below the d -band threshold are very short due to the large DOS. If the hole lifetimes were larger, then fewer secondary electrons would be generated, but with a longer delay after the creation of the electron-hole pair by the laser pulse. A longer delay will lead to the observation of a longer relaxation time in the excited state when secondary-electron contributions are important.

The interpretation given here that the non-monotonous feature in the lifetime in Cu is due to secondary (Auger) electrons has raised some controversy in the literature.^{7–9,11,12} While Knoesel *et al.*⁹ interpret their data by contributions from Auger electrons at intermediate-state energies above the d -band peak, Petek *et al.*¹² argue that secondary electrons make no significant contribution to the signal above $E - E_F = 1.5$ eV (for photon energy $h\nu = 3.1$ eV). The argument is based on a temperature-dependent delayed rise in the 2PPE signal as a function of time delay between the laser pulses, which is observed below and immediately above the d -band peak at $E - E_F = 0.9$ eV, but which vanishes above $E - E_F = 1.5$ eV and in the region of the peak. The temperature-dependent delayed rise is interpreted as a contribution from Auger electrons, which agrees with our interpretation of the feature in the lifetime. In Ref. 12, the fact that the delayed rise vanishes above 1.5 eV is taken as evidence that Auger electrons are absent in this energy region. In contrast to this conclusion, our calculations show significant contributions from secondary electrons up to about $E - E_F = 2.5$ eV (compare the relaxation times without [curve *b*] and with [curve *c*] secondary electrons in Fig. 3). We argue in the following that the absence of a resolvable second peak in the 2PPE signal is no evidence for the absence of Auger electrons. Thus the results of Ref. 12 are not in contradiction with our results. One would observe a second peak with a delay given by the hole lifetime at the d -band peak if all Auger electrons were created at a fixed rate corresponding to this hole lifetime. However, Auger electrons are also created by the filling of holes deeper in the d band with energies up to $h\nu$. These deep holes have shorter lifetimes than the ones at the top of the d band. Thus they lead to secondary-electron contributions to the dynamics in the intermediate state with a smaller delay time. The fact that holes with different lifetimes contribute to the secondary-electron dynamics makes it difficult to observe a resolvable second peak with a fixed delay corresponding to the lifetime at the d -band peak. Thus in our view, the measurements reported in Refs. 11,12 are not in contradiction with the interpretation of the non-monotonous feature in the relaxation time given in by us and in Ref. 9.

In Figs. 9 and 10 we compare experimental and theoretical results for the spin-averaged relaxation time τ and the ratio $\tau_\uparrow/\tau_\downarrow$ of majority and minority relaxation time for the ferromagnetic transition metals Fe, Co, and Ni. The discrepancies between experimental and theoretical results indicate that both DOS and Coulomb matrix elements play a role. Note, theoretical results refer to relaxation times of the distribution including secondary-electron effects. Transport effects have been neglected here in view of the fact that they cause only minor changes in the relaxation time of the transition metals, see Fig. 5.

First, the results calculated with $M = 0.8$ eV for all the transition metals are shown by the curves *a* in Figs. 9 and 10. The difference in the calculated relaxation times for Fe, Co, Ni, and Cu is then only due to the different DOS used as input for the calculation. Note, the calculated relaxation time is smaller than the experimental one in Co and Ni, while it is larger in Fe. The calculated ratio $\tau_\uparrow/\tau_\downarrow$ is larger in Co and Ni than the experimental one, but it is

smaller in Fe.

Secondly, in curves *b*, we show results of calculations using again $M = 0.8$ eV, but the reduced value $|M^{\uparrow\uparrow}/M^{\uparrow\downarrow}| = 0.5$. One expects that the matrix element $M^{\uparrow\uparrow}$ for scattering of parallel spins is smaller than $M^{\uparrow\downarrow}$ for antiparallel spins, since electrons with parallel spins avoid each other due to the Pauli exclusion principle.⁴⁶ The ratio $\tau_{\uparrow}/\tau_{\downarrow}$ is strongly reduced in Co and Ni, while it is increased in Fe, which leads to satisfactory agreement for $\tau_{\uparrow}/\tau_{\downarrow}$ between experimental and theoretical results. The spin-averaged relaxation time is not strongly affected by the value of $|M^{\uparrow\uparrow}/M^{\uparrow\downarrow}|$.

Thirdly, we take into account different Coulomb matrix elements M for the various metals, while we still use $|M^{\uparrow\uparrow}/M^{\uparrow\downarrow}| = 0.5$. The results are given by the curves *c* in Figs. 9 and 10. For Co and Ni we use $M = 0.4$ eV, while for Fe we take $M = 1.0$ eV. The use of these values for M leads to reasonable agreement between theoretical and experimental results for both the spin-averaged relaxation time and the ratio $\tau_{\uparrow}/\tau_{\downarrow}$.

Different Coulomb matrix elements in Fe, Co, Ni, and Cu are mainly caused by the influence of *d* electrons. Note, while in isolated atoms, Coulomb matrix elements do not vary much from Cu to Fe,⁴⁷ in solids the band character, the position of the *d* band, and the screening of *d* electrons are expected to change this. The screened Coulomb matrix elements for scattering between Bloch states with wave vectors \mathbf{k}_i in bands α_i is given by

$$M_{3;4}^{1;2} = \int d^3r d^3r' \psi_{\mathbf{k}_1\alpha_1}^*(\mathbf{r}) \psi_{\mathbf{k}_2\alpha_2}^*(\mathbf{r}') \frac{e^2}{\varepsilon(|\mathbf{r} - \mathbf{r}'|, \omega)} \frac{1}{|\mathbf{r} - \mathbf{r}'|} \psi_{\mathbf{k}_3\alpha_3}(\mathbf{r}) \psi_{\mathbf{k}_4\alpha_4}(\mathbf{r}'). \quad (11)$$

Here, ε is the dielectric function. The Coulomb matrix elements are of course influenced by *d* electrons, since their wave functions are more localized and also since they contribute to the screening of the Coulomb potential. The strong localization of *d* electrons leads to smaller overlap with *sp*-electron wave functions and therefore to smaller transition matrix elements when $sp \rightarrow d$ transitions are involved as compared to matrix elements involving $sp \rightarrow sp$ transitions. Note, the *d*-electron wave functions get more localized from Fe to Cu. The additional screening of *d* electrons is contained in the dielectric function $\varepsilon(|\mathbf{r} - \mathbf{r}'|, \omega)$, where ω is the energy transferred in the transition. Somewhat depending on ω , *d* electrons closer to the Fermi energy contribute mainly to screening. In the static limit ($\omega \rightarrow 0$), the Lindhard dielectric function for a free electron gas reduces to $\varepsilon(q) = 1 + k_0^2/q^2$ such that the screened Coulomb interaction in real space takes the form $V(r) = \frac{e^2}{r} e^{-k_0 r}$. In the Thomas-Fermi approximation, the screening wave vector is directly related to the DOS at the Fermi level,²⁴ $k_0 = 4\pi e^2 \rho(E_F)$. In the case of transition metals, the expressions are not strictly valid because *d* electrons are not free-electron-like. Although the quantitative contribution of *d* electrons to screening is not well-known, qualitatively it is clear that a higher DOS near the Fermi level leads to stronger screening. This may explain that the screened Coulomb matrix element in Co and Ni with many *d* electrons close to the Fermi energy is smaller than the one in Cu with nearly no *d* electrons close to the Fermi energy. For larger energy transfer ω , also electrons further away from the Fermi energy contribute to screening. Then ultimately the total number of *d* electrons influences screening. This could be the reason why Fe, which has fewer *d* electrons, has a larger Coulomb matrix element than Co, Ni, and Cu.

After completion of our study we noted that the influence of *d* electrons on the lifetime of low-energy electrons in noble and transition metals has also been studied recently in Refs. 16 and 18. Zarate *et al.*¹⁶ have studied the effect of DOS and Coulomb matrix elements on the lifetime in noble metals and ferromagnetic Co using simple approximations for the DOS and constant matrix elements. The golden-rule approach for the calculation of the scattering rates is equivalent to the method used by us for the calculation of the rate $\frac{\partial f_{Ea}}{\partial t}|_{e \rightarrow e}^{\text{out}}$. Choosing different matrix elements for transitions with a different number of *sp* and *d* states, Zarate *et al.* obtain good agreement with experimental results for the relaxation time in Co.¹³ It is important to clarify the influence of *sp* and *d* states on Coulomb matrix elements and lifetimes in transition metals as was done in Ref. 16. For better comparison with experiments, further work along these lines including also the contribution of secondary electrons would be interesting. Campillo *et al.*¹⁸ have calculated lifetimes in Cu from the self-energy within the GW approximation. Using the density-functional theory for the determination of the electronic structure and the RPA for the calculation of the screened Coulomb interaction, they found important contributions of *d* electrons to the lifetime via screening, localization of the wave function and DOS effects. The single-electron lifetime for Cu calculated by us with Coulomb matrix element $M = 0.8$ eV (see curve *b* in Fig.3) is in good agreement with the lifetime calculated in Ref. 18.

VI. CONCLUSION

We have presented experimental and theoretical results for the dynamics of excited electrons in Cu, Fe, Co, and Ni.

In the theoretical part, we have presented a model for the dynamics of excited electrons including effects of the optical excitation, electron-electron scattering, generation of secondary electrons and transport of excited carriers out of the detection region. The electron-electron scattering rates were calculated using realistic DOS for the different metals and energy-independent Coulomb matrix elements.

For Cu, we have presented theoretical and experimental results which show the influence of secondary electrons and transport effects on the observed relaxation time. The non-monotonous behavior in the relaxation time obtained in the calculation is in qualitative agreement with experiments. It seems desirable to achieve a better quantitative agreement for this structure in order to draw definitive conclusions about the role played by secondary electrons.

Experimental results for the spin-dependent relaxation time for all of the 3d transition metals Fe, Co, and Ni were presented. The relation of the magnitude of the relaxation time is $\tau_{\text{Fe}} < \tau_{\text{Ni}} < \tau_{\text{Co}}$. The ratio $\tau_{\uparrow}/\tau_{\downarrow}$ is found to lie between 1 and 2 for the three metals. Transport effects were found to be only of minor importance for the transition metals in the discussed energy range, whereas they are important for Cu. We found for the calculated relaxation time that $\tau_{\text{Ni}} < \tau_{\text{Co}} < \tau_{\text{Fe}}$ at energies below $E - E_F = 1$ eV if we use $M = 0.8$ eV, in contrast to experimental results.

The comparison of experimental and theoretical results shows that DOS effects alone do not explain the magnitude of the relaxation time for the various transition metals observed in experiments. The differences between the calculation using the same Coulomb matrix element for Fe, Co, and Ni and experiments reveal that Coulomb-matrix-element effects are important. Reasonable agreement between calculated results and experiment for the magnitude of the spin-averaged relaxation time is found for values $M = 0.8$ eV for Cu, $M = 0.4$ eV for Co and Ni and $M = 1.2$ eV for Fe. The ratio $|M^{\uparrow\uparrow}/M^{\uparrow\downarrow}| = 0.5$ leads to satisfactory agreement for the ratio $\tau_{\uparrow}/\tau_{\downarrow}$.

As an outlook for further studies, we conclude that more detailed calculations have to include a first-principles calculation of the Coulomb interaction matrix elements. Notably one has to take into account the screening by the d electrons, the influence of the localized d -electron wave functions on the Coulomb matrix elements, and the energy dependence of the matrix elements. Further studies of the influence of the optical excitation, for example the influence of the photon energy and the polarization of the incoming light on the observed dynamics, are needed. Also the influence of the hole lifetime on the calculated relaxation times should be investigated. The rate of filling of d -band holes influences the time evolution of the distribution and hence also the observed relaxation time for levels above the Fermi energy via the generation of secondary electrons. Hole lifetimes have been observed in recent experiments on Cu,⁴⁸ and their effect on two-photon photoemission has also been considered in a recent theoretical work.¹⁰

ACKNOWLEDGMENTS

R.K. and K.B. gratefully acknowledge financial support by Deutsche Forschungsgemeinschaft (SFB 290). R.B. and M.A. would like to thank all co-workers who contributed to the experimental work described here, in particular M. Bauer, S. Pawlik, W. Weber, and D. Oberli. H.C. Siegmann is thanked for many stimulating discussions.

APPENDIX A: ELECTRON-ELECTRON SCATTERING RATES

We derive here the electron-electron scattering rates. We extend an earlier treatment in order to calculate the scattering rates into a level as well as out of a level for a given non-equilibrium distribution function.¹⁵

The scattering rate out of the state with momentum \mathbf{p} , band α (designating sp or d -like wave function) and spin σ is given in first order time-dependent perturbation theory (golden rule) by:

$$\begin{aligned} \frac{\partial f_{\mathbf{p}\alpha\sigma}}{\partial t} \bigg|_{\text{e-e}}^{\text{out}} = & -f_{\mathbf{p}\alpha\sigma} \frac{2\pi}{\hbar} \sum_{\mathbf{p}'\mathbf{k}\mathbf{k}',\beta\gamma\delta} \left\{ \frac{1}{2} f_{\mathbf{k}\gamma\sigma} (1 - f_{\mathbf{p}'\beta\sigma}) (1 - f_{\mathbf{k}'\delta\sigma}) \left| M_{\mathbf{p}'\beta\sigma; \mathbf{k}'\delta\sigma}^{\mathbf{p}\alpha\sigma; \mathbf{k}\gamma\sigma} - M_{\mathbf{k}'\delta\sigma; \mathbf{p}'\beta\sigma}^{\mathbf{p}\alpha\sigma; \mathbf{k}\gamma\sigma} \right|^2 \right. \right. \\ & \times \delta(E_{\mathbf{p}\alpha\sigma} + E_{\mathbf{k}\gamma\sigma} - E_{\mathbf{p}'\beta\sigma} - E_{\mathbf{k}'\delta\sigma}) \\ & + f_{\mathbf{k}\gamma\bar{\sigma}} (1 - f_{\mathbf{p}'\beta\sigma}) (1 - f_{\mathbf{k}'\delta\bar{\sigma}}) \left| M_{\mathbf{p}'\beta\sigma; \mathbf{k}'\delta\bar{\sigma}}^{\mathbf{p}\alpha\sigma; \mathbf{k}\gamma\bar{\sigma}} \right|^2 \\ & \left. \left. \times \delta(E_{\mathbf{p}\alpha\sigma} + E_{\mathbf{k}\gamma\bar{\sigma}} - E_{\mathbf{p}'\beta\sigma} - E_{\mathbf{k}'\delta\bar{\sigma}}) \right\} . \right. \end{aligned} \quad (\text{A1})$$

The first term describes triplet scattering, where an electron with spin σ interacts with a second electron of the same spin. There are two possible processes for the same final state, which differ in the momentum exchanged in the process. The factor 1/2 in the sum has to be included to avoid counting the same process twice. The second term describes singlet scattering, i.e. scattering of two electrons with opposite spin (σ and $\bar{\sigma}$).

The scattering rate can be written in a more suggestive form after some manipulations. The singlet term is split in two equal terms (each getting a factor of 1/2) and in one of the terms, we exchange $\mathbf{p}'\beta$ and $\mathbf{k}'\delta$. Then the sum over \mathbf{p}' is done first (to simplify we replace the different energy-conserving delta functions by δ_E):

$$\begin{aligned} \left. \frac{\partial f_{\mathbf{p}\alpha\sigma}}{\partial t} \right|_{\text{e-e}}^{\text{out}} &= -\frac{1}{2} f_{\mathbf{p}\alpha\sigma} \sum_{\mathbf{p}',\beta} \left\{ (1 - f_{\mathbf{p}'\beta\sigma}) \frac{2\pi}{\hbar} \sum_{\mathbf{k}\mathbf{k}',\gamma\delta} \left(f_{\mathbf{k}\gamma\sigma} (1 - f_{\mathbf{k}'\delta\sigma}) \left| M_{\mathbf{p}'\beta\sigma; \mathbf{k}'\delta\sigma}^{\mathbf{p}\alpha\sigma; \mathbf{k}\gamma\sigma} - M_{\mathbf{k}'\delta\sigma; \mathbf{p}'\beta\sigma}^{\mathbf{p}\alpha\sigma; \mathbf{k}\gamma\sigma} \right|^2 \delta_E \right. \right. \\ &\quad \left. \left. + f_{\mathbf{k}\gamma\bar{\sigma}} (1 - f_{\mathbf{k}'\delta\bar{\sigma}}) \left| M_{\mathbf{p}'\beta\sigma; \mathbf{k}'\delta\bar{\sigma}}^{\mathbf{p}\alpha\sigma; \mathbf{k}\gamma\bar{\sigma}} \right|^2 \delta_E \right) \right. \\ &\quad \left. + (1 - f_{\mathbf{p}'\beta\sigma}) \frac{2\pi}{\hbar} \sum_{\mathbf{k}\mathbf{k}',\gamma\delta} f_{\mathbf{k}\gamma\bar{\sigma}} (1 - f_{\mathbf{k}'\delta\bar{\sigma}}) \left| M_{\mathbf{k}'\delta\sigma; \mathbf{p}'\beta\bar{\sigma}}^{\mathbf{p}\alpha\sigma; \mathbf{k}\gamma\bar{\sigma}} \right|^2 \delta_E \right\}. \end{aligned} \quad (\text{A2})$$

The second summation defines two separate scattering rates:

$$\begin{aligned} \omega(\mathbf{p}\alpha\sigma, \mathbf{p}'\beta\sigma) &= \frac{2\pi}{\hbar} \sum_{\mathbf{k}\mathbf{k}',\gamma\delta} \left(f_{\mathbf{k}\gamma\sigma} (1 - f_{\mathbf{k}'\delta\sigma}) \left| M_{\mathbf{p}'\beta\sigma; \mathbf{k}'\delta\sigma}^{\mathbf{p}\alpha\sigma; \mathbf{k}\gamma\sigma} - M_{\mathbf{k}'\delta\sigma; \mathbf{p}'\beta\sigma}^{\mathbf{p}\alpha\sigma; \mathbf{k}\gamma\sigma} \right|^2 \delta_E \right. \right. \\ &\quad \left. \left. + f_{\mathbf{k}\gamma\bar{\sigma}} (1 - f_{\mathbf{k}'\delta\bar{\sigma}}) \left| M_{\mathbf{p}'\beta\sigma; \mathbf{k}'\delta\bar{\sigma}}^{\mathbf{p}\alpha\sigma; \mathbf{k}\gamma\bar{\sigma}} \right|^2 \delta_E \right) , \right. \end{aligned} \quad (\text{A3})$$

$$\omega(\mathbf{p}\alpha\sigma, \mathbf{p}'\beta\bar{\sigma}) = \frac{2\pi}{\hbar} \sum_{\mathbf{k}\mathbf{k}',\gamma\delta} f_{\mathbf{k}\gamma\bar{\sigma}} (1 - f_{\mathbf{k}'\delta\bar{\sigma}}) \left| M_{\mathbf{k}'\delta\sigma; \mathbf{p}'\beta\bar{\sigma}}^{\mathbf{p}\alpha\sigma; \mathbf{k}\gamma\bar{\sigma}} \right|^2 \delta_E. \quad (\text{A4})$$

The first rate gives the probability per unit time that an electron scatters out of the level $\mathbf{p}\alpha\sigma$ and by the same scattering process, another electron scatters into the level $\mathbf{p}'\beta\sigma$. The incoming and outgoing electrons have the same spin. This rate is therefore called the "non-flip" rate. The second rate gives the probability per unit time that an electron scatters out of $\mathbf{p}\alpha\sigma$ and another electron scatters into $\mathbf{p}'\beta\bar{\sigma}$. This rate is called the "flip" rate. In both processes, the total spin is conserved. The notations "flip" and "non-flip" rates refer only to the two levels that are considered.

Using these definitions, the rate for scattering out of $\mathbf{p}\alpha\sigma$ can be written as:

$$\left. \frac{\partial f_{\mathbf{p}\alpha\sigma}}{\partial t} \right|_{\text{e-e}}^{\text{out}} = -\frac{1}{2} f_{\mathbf{p}\alpha\sigma} \sum_{\mathbf{p}',\beta} \left\{ (1 - f_{\mathbf{p}'\beta\sigma}) \omega(\mathbf{p}\alpha\sigma, \mathbf{p}'\beta\sigma) + (1 - f_{\mathbf{p}'\beta\bar{\sigma}}) \omega(\mathbf{p}\alpha\sigma, \mathbf{p}'\beta\bar{\sigma}) \right\}. \quad (\text{A5})$$

In the same manner, the rate for scattering into $\mathbf{p}\alpha\sigma$ is given by

$$\left. \frac{\partial f_{\mathbf{p}\alpha\sigma}}{\partial t} \right|_{\text{e-e}}^{\text{in}} = \frac{1}{2} (1 - f_{\mathbf{p}\alpha\sigma}) \sum_{\mathbf{p}',\beta} \left\{ f_{\mathbf{p}'\beta\sigma} \omega(\mathbf{p}'\beta\sigma, \mathbf{p}\alpha\sigma) + f_{\mathbf{p}'\beta\bar{\sigma}} \omega(\mathbf{p}'\beta\bar{\sigma}, \mathbf{p}\alpha\sigma) \right\}. \quad (\text{A6})$$

Now we convert the sums over momenta into integrals over energies. This approximation is called the random- \mathbf{k} approximation and is based on the assumption that the scattering in \mathbf{k} space is so effective that the dependence on the direction of the momenta is averaged out. The conversion to \mathbf{k} -averaged quantities is done in the following way:

$$\sum_{\mathbf{k}} f_{\mathbf{k}\alpha\sigma} \rightarrow \int_{-\infty}^{\infty} dE \rho_{E\alpha\sigma} f_{E\alpha\sigma}.$$

Each \mathbf{k} sum leads to a factor of the density of states (DOS), $\rho_{E\alpha\sigma}$. For ease of notation, products of distribution functions and densities of states are defined in the following way:

$$e_{E\alpha\sigma} = \rho_{E\alpha\sigma} f_{E\alpha\sigma}, \quad h_{E\alpha\sigma} = \rho_{E\alpha\sigma} (1 - f_{E\alpha\sigma}). \quad (\text{A7})$$

The notation is chosen since $e_{E\alpha\sigma}$ stands for the number of electrons, $h_{E\alpha\sigma}$ for the number of holes at energy E , in band α , with spin σ . Using the replacements $\mathbf{p} \rightarrow E$ and $\mathbf{p}' \rightarrow E'$, the \mathbf{k} -averaged form of the scattering rate out of and into the state $E\alpha\sigma$ are then given by:

$$\left. \frac{\partial f_{E\alpha\sigma}}{\partial t} \right|_{\text{e-e}}^{\text{out}} = -f_{E\alpha\sigma} \frac{1}{2} \sum_{\beta} \int_{-\infty}^{\infty} dE' \left\{ h_{E'\beta\sigma} W(E\alpha\sigma, E'\beta\sigma) + h_{E'\beta\bar{\sigma}} W(E\alpha\sigma, E'\beta\bar{\sigma}) \right\}, \quad (\text{A8})$$

$$\left. \frac{\partial f_{E\alpha\sigma}}{\partial t} \right|_{\text{e-e}}^{\text{in}} = (1 - f_{E\alpha\sigma}) \frac{1}{2} \sum_{\beta} \int_{-\infty}^{\infty} dE' \left\{ e_{E'\beta\sigma} W(E'\beta\sigma, E\alpha\sigma) + e_{E'\beta\bar{\sigma}} W(E'\beta\bar{\sigma}, E\alpha\sigma) \right\}. \quad (\text{A9})$$

For the \mathbf{k} -averaged form of the nonflip and flip scattering rates, we take $\mathbf{k} \rightarrow \varepsilon$ and $\mathbf{k}' \rightarrow \varepsilon'$ and perform the integral over ε' . Because of the δ -function, we can replace ε' by $\varepsilon + \omega$ with $\omega = E - E'$:

$$W(E\alpha\sigma, E'\beta\sigma) = \frac{2\pi}{\hbar} \sum_{\gamma\delta} \int_{-\infty}^{\infty} d\varepsilon \left(e_{\varepsilon\gamma\sigma} h_{\varepsilon+\omega, \delta\sigma} \left| M_{E'\beta\sigma; \varepsilon+\omega, \delta\sigma}^{E\alpha\sigma; \varepsilon\gamma\sigma} - M_{\varepsilon+\omega, \delta\sigma; E'\beta\sigma}^{E\alpha\sigma; \varepsilon\gamma\sigma} \right|^2 \right. \\ \left. + e_{\varepsilon\gamma\bar{\sigma}} h_{\varepsilon+\omega, \delta\bar{\sigma}} \left| M_{E'\beta\sigma; \varepsilon+\omega, \delta\bar{\sigma}}^{E\alpha\sigma; \varepsilon\gamma\bar{\sigma}} \right|^2 \right), \quad (\text{A10})$$

$$W(E\alpha\sigma, E'\beta\bar{\sigma}) = \frac{2\pi}{\hbar} \sum_{\gamma\delta} \int_{-\infty}^{\infty} d\varepsilon e_{\varepsilon\gamma\bar{\sigma}} h_{\varepsilon+\omega, \delta\sigma} \left| M_{\varepsilon+\omega, \delta\sigma; E'\beta\bar{\sigma}}^{E\alpha\sigma; \varepsilon\gamma\bar{\sigma}} \right|^2. \quad (\text{A11})$$

Up to this point we keep the general dependence of the Coulomb matrix elements on energy, band label and the spin of the four states involved in the transition. Since an *ab-initio* calculation of the Coulomb matrix elements from the wave functions is beyond the scope of this work, we will, from now on, use a simple parametrization of the matrix elements.

The first approximation is that we do not further distinguish between states of *sp* or *d* symmetry in the matrix element. This is done for two reasons. First, it is difficult to make a statement about the dependence of the matrix elements on the character of the states involved in the transition without actually calculating the matrix elements from the wave functions. Secondly, we performed tests with different matrix elements depending on the *sp* or *d* character of the states involved and have not found qualitative changes in the results. However, we are aware that, in general, the dependence on the band label may be significant and we wish to study this topic in a forthcoming work. A dependence of the matrix elements on the *sp* or *d* character of the states involved has been shown for example in Ref. 49. Also, transmission experiments in the range of 5–10 eV above the Fermi level suggest a different cross-section for *sp* and *d* states.^{20,35} When the dependence of the matrix elements on the band label is neglected, in Eqs. (A8–A11), the sums over the band labels β , γ and δ can be performed and instead of the partial DOS $\rho_{E\alpha\sigma}$ one obtains the total DOS $\rho_{E\sigma}$. Thus, the form of the equations remains the same when the partial DOS is replaced by the total DOS.

The second approximation regarding the matrix elements is that we neglect the energy dependence. This approximation is based on the assumption that in the range of a few eV from the Fermi energy, the energy dependence of the matrix elements is weak. As in the case of the dependence on the band label, the calculation of the energy dependence of the Coulomb matrix elements is beyond the scope of the present work. It will be subject of further studies. When using energy-independent matrix elements, one is faced with the problem that in Eq. (A10), there is an interference term between two matrix elements with different energy arguments. This term appears in the case of scattering between two electrons of equal spin (triplet scattering). We treat the interference term in the following way. Before introducing constant matrix elements, we expand the modulus square; in the following, we neglect the interference term:

$$|M_1^{\sigma\sigma} - M_2^{\sigma\sigma}|^2 = |M_1^{\sigma\sigma}|^2 + |M_2^{\sigma\sigma}|^2 - [M_1^{\sigma\sigma}(M_2^{\sigma\sigma})^* + \text{c.c.}] \approx |M_1^{\sigma\sigma}|^2 + |M_2^{\sigma\sigma}|^2 = 2|M^{\sigma\sigma}|^2. \quad (\text{A12})$$

For simplicity, we have denoted the matrix elements with different energy arguments by $M_1^{\sigma\sigma}$ and $M_2^{\sigma\sigma}$. After expanding the modulus square and neglecting the interference term, in the last step we drop the energy index and use constant matrix elements $M^{\sigma\sigma} = M_1^{\sigma\sigma} = M_2^{\sigma\sigma}$. The approximation of neglecting the interference term was also made by Penn *et al.*¹⁵ For a non-magnetic metal with spin-independent DOS, in Eqs. (A8–A9) for the scattering rates, this leads to an equal contribution from scattering among electrons with equal and opposite spin. The Coulomb matrix elements for triplet and singlet scattering are denoted by $M^{\sigma\sigma}$ and $M^{\sigma\bar{\sigma}}$. We use $M^{\uparrow\uparrow} = M^{\downarrow\downarrow}$ and $M^{\uparrow\downarrow} = M^{\downarrow\uparrow}$.

After these approximations, the simplified equations for the scattering rates used in the calculations are:

$$\frac{\partial f_{E\sigma}}{\partial t} \bigg|_{\text{e-e}}^{\text{out}} = -f_{E\sigma} \frac{1}{2} \int_{-\infty}^{\infty} dE' \left\{ h_{E'\sigma} W(E\sigma, E'\sigma) + h_{E'\bar{\sigma}} W(E\sigma, E'\bar{\sigma}) \right\}, \quad (\text{A13})$$

$$\frac{\partial f_{E\sigma}}{\partial t} \bigg|_{\text{e-e}}^{\text{in}} = (1 - f_{E\sigma}) \frac{1}{2} \int_{-\infty}^{\infty} dE' \left\{ e_{E'\sigma} W(E'\sigma, E\sigma) + e_{E'\bar{\sigma}} W(E'\bar{\sigma}, E\sigma) \right\}, \quad (\text{A14})$$

$$W(E\sigma, E'\sigma) = \frac{2\pi}{\hbar} \int_{-\infty}^{\infty} d\varepsilon \left(e_{\varepsilon\sigma} h_{\varepsilon+\omega, \sigma} 2|M^{\uparrow\uparrow}|^2 + e_{\varepsilon\bar{\sigma}} h_{\varepsilon+\omega, \bar{\sigma}} |M^{\uparrow\downarrow}|^2 \right), \quad (\text{A15})$$

$$W(E\sigma, E'\bar{\sigma}) = \frac{2\pi}{\hbar} \int_{-\infty}^{\infty} d\varepsilon e_{\varepsilon\bar{\sigma}} h_{\varepsilon+\omega, \sigma} |M^{\uparrow\downarrow}|^2. \quad (\text{A16})$$

To discuss the magnitude and spin dependence of the lifetime, it is convenient to introduce two parameters, M^2 for the average matrix element squared and m for the ratio of $M^{\uparrow\uparrow}$ and $M^{\uparrow\downarrow}$:

$$M^2 = \frac{|M^{\uparrow\uparrow}|^2 + |M^{\uparrow\downarrow}|^2}{2}, \quad m = \frac{|M^{\uparrow\uparrow}|}{|M^{\uparrow\downarrow}|}.$$

* Corresponding author. Electronic address: roland.knorren@physik.fu-berlin.de

† Present address: Institute for Laser and Plasma Physics, University of Essen, D-45117 Essen, Germany.

- ¹ C. A. Schmuttenmaer, M. Aeschlimann, H.E. Elsayed-Ali, R.J.D. Miller, D.A. Mantell, J.Cao, and Y. Gao, Phys. Rev. B **50**, 8957 (1994).
- ² T. Hertel, E. Knoesel, M. Wolf, and G. Ertl, Phys. Rev. Lett. **76**, 535 (1996).
- ³ J.J. Quinn, Phys. Rev. **126**, 1453 (1962).
- ⁴ M. Aeschlimann, M. Bauer, and S. Pawlik, Chem. Phys. **205**, 127 (1996).
- ⁵ S. Ogawa, H. Nagano, and H. Petek, Phys. Rev. B **55**, 10869 (1997).
- ⁶ E. Knoesel, A. Hotzel, T. Hertel, M. Wolf and G. Ertl, Surf. Sci. **368**, 76 (1996).
- ⁷ S. Pawlik, M. Bauer and M. Aeschlimann, Surf. Sci. **377-379**, 206 (1997).
- ⁸ J. Cao, Y. Gao, R.J.D. Miller, H.E. Elsayed-Ali, and D.A. Mantell, Phys. Rev. B **56**, 1099 (1997).
- ⁹ E. Knoesel, A. Hotzel, and M. Wolf, Phys. Rev. B **57**, 12812 (1998).
- ¹⁰ M. Sakaue, H. Kasai, and A. Okiji, J. Phys. Soc. Jpn. **68**, 720 (1999).
- ¹¹ H. Petek and S. Ogawa, Prog. Surf. Sci. **56**, 239 (1997).
- ¹² H. Petek, H. Nagano, and S. Ogawa, Appl. Phys. B **68**, 369 (1999).
- ¹³ M. Aeschlimann, M. Bauer, S. Pawlik, W. Weber, R. Burgermeister, D. Oberli, and H.C. Siegmann, PRL **79**, 5158 (1997).
- ¹⁴ M. Aeschlimann, R. Burgermeister, S. Pawlik, M. Bauer, D. Oberli, and W. Weber, J. Elec. Spectros. **88-91**, 179 (1998).
- ¹⁵ D.R. Penn, S.P. Apell, and S.M. Girvin, Phys. Rev. B **32**, 7753 (1985).
- ¹⁶ E. Zarate, P. Apell, and P.M. Echenique, Phys. Rev. B **60**, 2326 (1999).
- ¹⁷ E.V. Chulkov, I. Sarria, V.M. Silkin, J.M. Pitarke, and P.M. Echenique, Phys. Rev. Lett. **80**, 4947 (1998).
- ¹⁸ I. Campillo, J.M. Pitarke, A. Rubio, E. Zarate, and P.M. Echenique, cond-mat/9907490.
- ¹⁹ S. Hüfner, in *Springer Series in Solid State Sciences*, edited by M. Cardona, P. Fulde, K. von Klitzing, H.-J. Queisser, Vol. 82, Ch. 7 (Springer, Berlin, Heidelberg, 1995).
- ²⁰ H.C. Siegmann, Surf. Sci. **307-309** 1076 (1994).
- ²¹ S. Ogawa, H. Nagano, H. Petek, and A. P. Heberle, Phys. Rev. Lett. **78**, 1339 (1997).
- ²² C. Timm and K.H. Bennemann, submitted to Phys. Rev. B (1999).
- ²³ H. Petek, H. Nagano, and S. Ogawa, Phys. Rev. Lett. **83**, 832 (1999).
- ²⁴ J.M. Ziman, *Principles of the Theory of Solids* (Cambridge University Press, 1972).
- ²⁵ V.L. Moruzzi, J.F. Janak, A.R. Williams, *Calculated Electronic Properties of Metals* (Pergamon, New York, 1978).
- ²⁶ W.A. Harrison, *Electronic Structure and the Properties of Solids* (Freeman, San Francisco, 1979).
- ²⁷ J. J. Quinn and R. A. Ferrell, Phys. Rev. **112**, 812 (1958).
- ²⁸ P.M. Echenique, J.M. Pitarke, E.V. Chulkov, and A. Rubio, cond-mat/9908126.
- ²⁹ D. A. Papaconstantopoulos, *Handbook of the Band Structure of Elemental Solids* (Plenum, New York, 1986).
- ³⁰ Densities of states were calculated by the FLAPW band structure program WIEN95 and were provided to us by J. Dewitz, private communication (1998).
- ³¹ H. Eckhardt, L. Fritzsche, and J. Noffke, J. Phys. F, Met. Phys. **14**, 97 (1984).
- ³² P.B. Johnson and R.W. Christy, Phys. Rev. B **6**, 4370 (1972); Phys. Rev. B **9**, 5056 (1974).
- ³³ R. Knorren and K.H. Bennemann, Appl. Phys. B **68**, 401 (1999).
- ³⁴ E. Knoesel, Ph.D. thesis, Freie Universität Berlin (1997).
- ³⁵ H.C. Siegmann, J. Phys., Condens. Matter **4** 8395 (1992).
- ³⁶ J. Kirschner, in *Polarized Electrons in Surface Physics*, edited by R. Feder (World Scientific, Singapore, 1985).
- ³⁷ W. Weber *et al.*, Phys. Rev. B **54**, 4075 (1996).
- ³⁸ P. Kramers *et al.*, Phys. Rev. Lett. **69**, 3674 (1992).
- ³⁹ J. Thomassen *et al.*, Phys. Rev. Lett. **69**, 3831, (1992).
- ⁴⁰ F. Scheurer *et al.*, Phys. Rev. B **48**, 9890 (1993).
- ⁴¹ R. Naik *et al.*, J. Magn. Magn. Mat. **121**, 60 (1993).
- ⁴² G. Bochi *et al.*, J. Appl. Phys. **75**, 6430, (1994).
- ⁴³ M. Bauer, S. Pawlik, and M. Aeschlimann, Phys. Rev. B **55**, 10040, (1997).
- ⁴⁴ M. Bauer, S. Pawlik, and M. Aeschlimann, Phys. Rev. B **60**, 5016 (1999).
- ⁴⁵ M. Bauer, S. Pawlik, R. Burgermeister, and M. Aeschlimann, Surf. Sci., **402-404**, 62 (1998).
- ⁴⁶ J. Friedel, in *Physics of Metals*, edited by J. M. Ziman, Vol. 1, Ch. 8 (Cambridge University Press, Cambridge, 1969).

⁴⁷ J.B. Mann, *Atomic Structure Calculations*, Los Alamos Sci. Lab. Rept. LA-3690 (1967).

⁴⁸ R. Matzdorf, A. Gerlach, F. Theilmann, G. Meister, and A. Goldmann, *Appl. Phys. B* **68**, 393 (1999).

⁴⁹ H. Ebert and V. Popescu, *Phys. Rev. B* **56**, 12 884 (1997).

TABLE I. Optical penetration depth λ_{opt} for $h\nu = 3 \text{ eV}$.³²

	Fe	Co	Ni	Cu
$\lambda_{\text{opt}} (\text{\AA})$	124	108	122	149

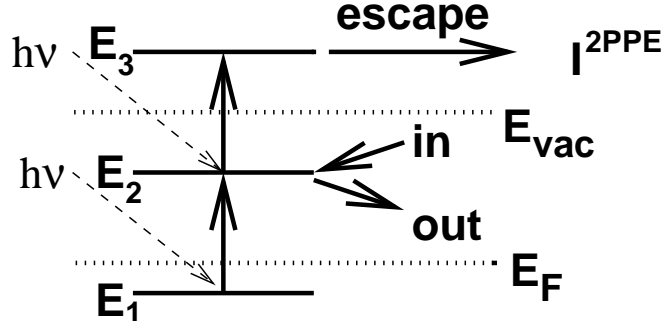


FIG. 1. Illustration of the monochromatic 2PPE process with initial state E_1 , intermediate state E_2 and final state E_3 . A first photon excites an electron from an initial level E_1 in the range between E_F and $E_F - h\nu$ into a level E_2 . The population $f(E_2, t)$ depends on the temporal pulse shape of the exciting laser and is time-dependent due to electron-electron interaction and transport of electrons out of the optically excited region into the bulk. A second photon excites an electron with energy E_2 into a state E_3 above the vacuum energy E_{vac} , from which it can contribute to the 2PPE intensity via $I^{\text{2PPE}}(E_3, t) \propto f(E_2, t)$.

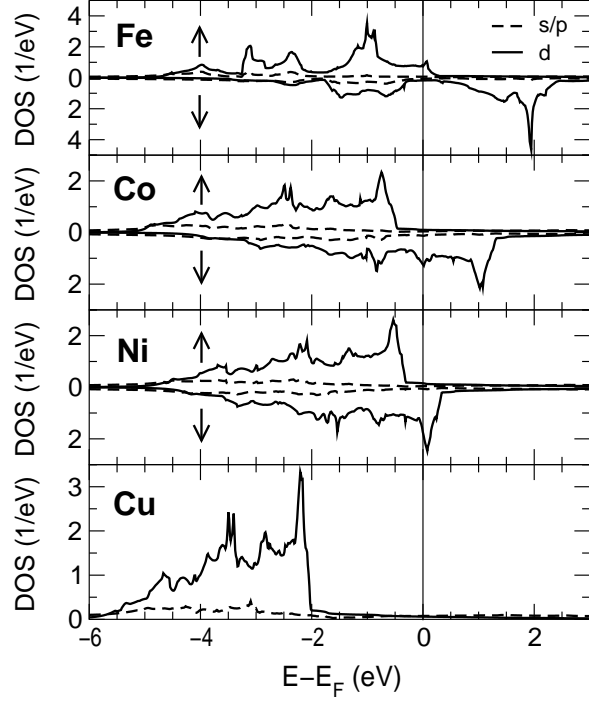


FIG. 2. LAPW density of states (DOS) used as input in the calculation of the electron-electron scattering rates in Eqs. (4–7).

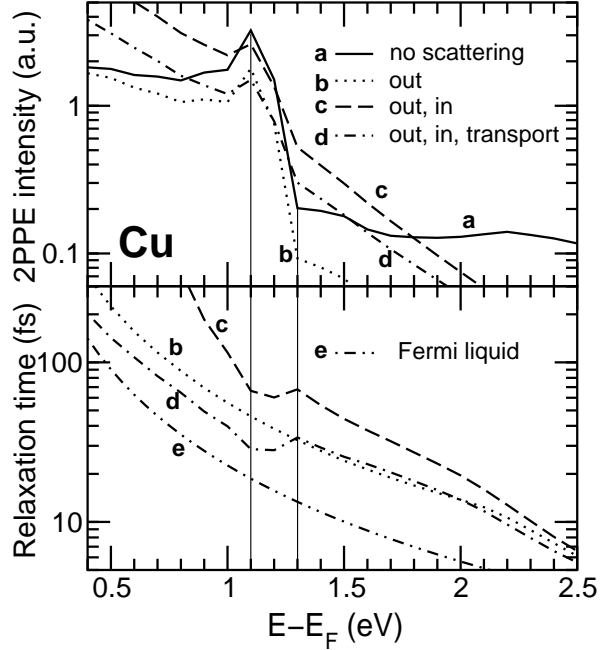


FIG. 3. Calculated 2PPE intensity and relaxation time of the excited electron distribution for Cu for photon energy $h\nu = 3.3$ eV. Curve *a* shows the 2PPE intensity if no scattering is present and reflects the distribution of optically excited electrons. Curve *b* gives the result if only scattering out of the intermediate level is kept in Eq. (2). Curve *c* is the result if scattering into the intermediate state (secondary electron effect) is also included. Curve *d* represents the case when the effect of transport is also taken into account. The relaxation time when only scattering out of the intermediate state is kept (curve *b*) is a single-electron lifetime and can be compared with the lifetime predicted by Fermi-liquid theory, shown in curve *e*. The other relaxation times are effective relaxation times of the distribution of excited electrons.

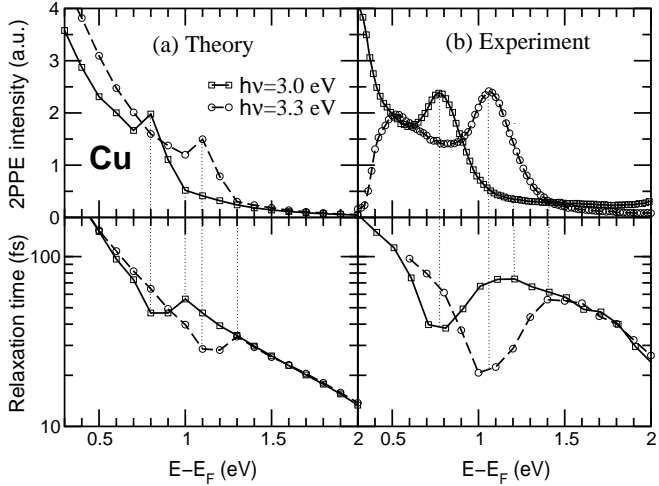


FIG. 4. Calculated (a) and measured (b) 2PPE intensity and relaxation time for Cu for photon energies $h\nu = 3.0$ and 3.3 eV. Calculations include secondary electrons and transport. Note the dependence of the relaxation time on photon energy, especially in the region of the peak in the intensity ($E - E_F = 0.7 - 1.3$ eV). The minimum in the relaxation time corresponds to the peak in the intensity and the maximum in the relaxation time corresponds to the d -band threshold, as indicated by the dotted lines, in agreement with several experiments.⁷⁻⁹

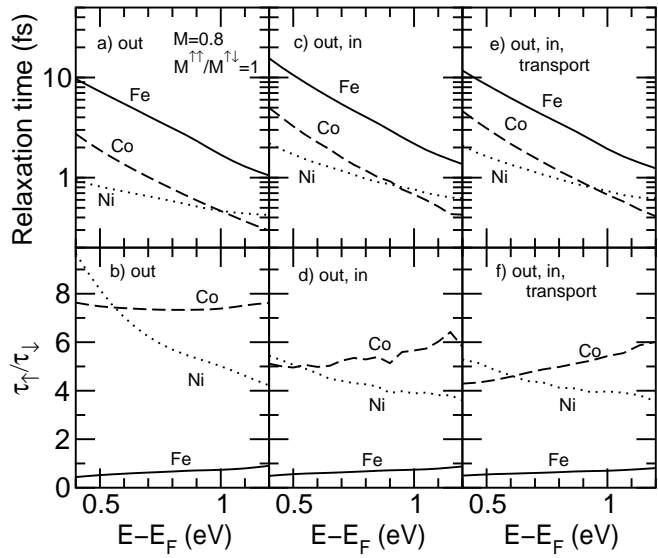


FIG. 5. Spin-averaged relaxation time of the distribution and ratio of relaxation times for majority and minority electrons. Results labelled *out* are single-electron lifetimes. Results (*out,in*) refer to relaxation times of the distribution including secondary electrons. Results (*out, in, transport*) also include transport. The same average Coulomb matrix element $M = 0.8$ eV and $|M^{\uparrow\uparrow}/M^{\uparrow\downarrow}| = 1$ is used.

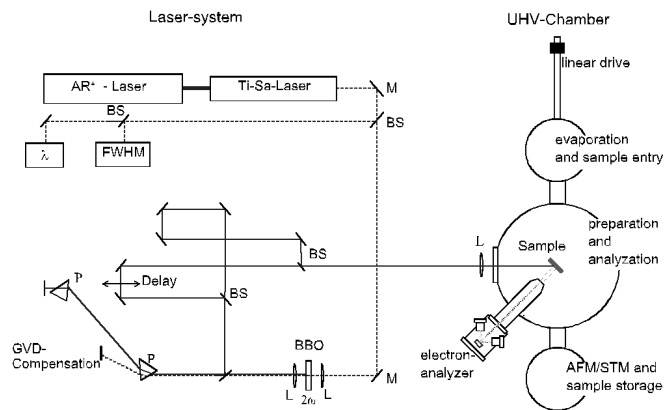


FIG. 6. Schematic view of the equal pulse correlation set-up for time resolved 2PPE.

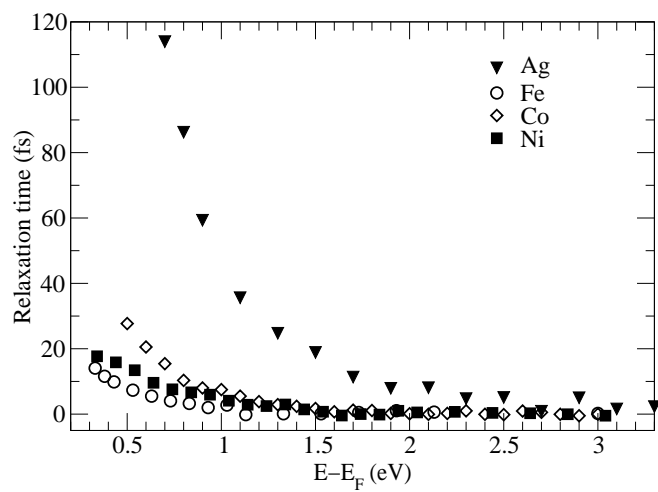


FIG. 7. Comparison of experimental relaxation time results for Ag and the three transition metals, Fe, Co, and Ni.

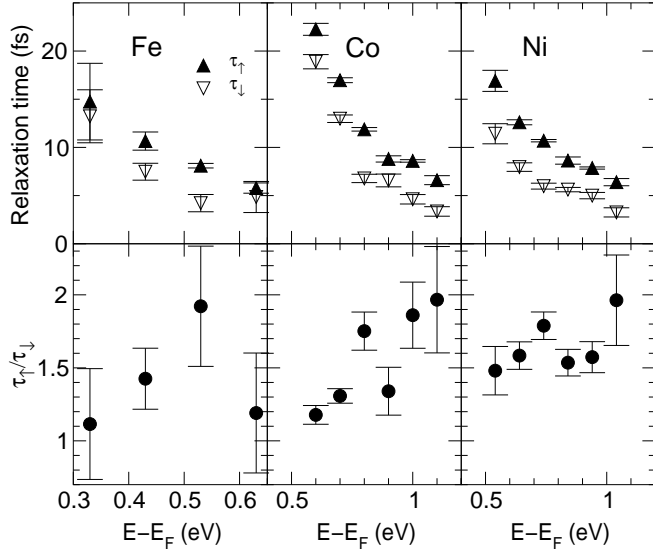


FIG. 8. Experimental results for the spin-resolved relaxation time τ_\uparrow and τ_\downarrow and the ratio $\tau_\uparrow/\tau_\downarrow$ of majority to minority relaxation time.

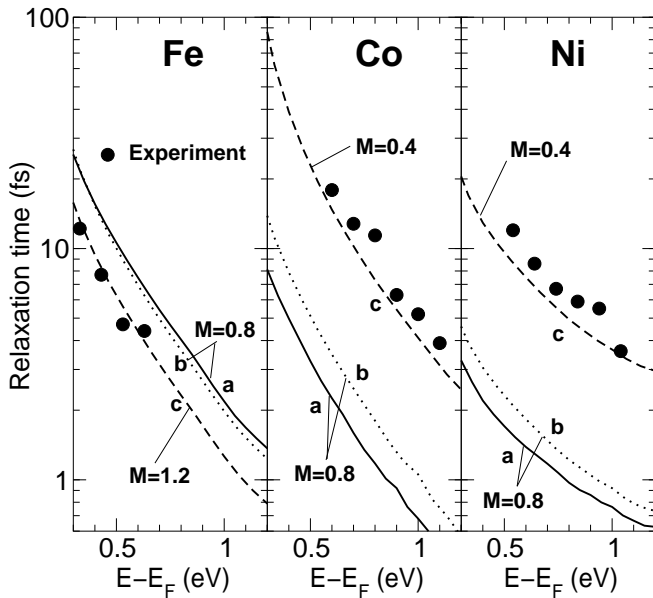


FIG. 9. Experimental and theoretical results for the spin-averaged relaxation time of the distribution. Calculations include secondary electron effects. Curve *a* shows results using Coulomb matrix element $M = 0.8$ eV and $|M^{\uparrow\uparrow}/M^{\uparrow\downarrow}| = 1$ for the various transition metals. Curve *b* gives results for the same M , but $|M^{\uparrow\uparrow}/M^{\uparrow\downarrow}| = 0.5$. Results using different values of M for the various transition metals and $|M^{\uparrow\uparrow}/M^{\uparrow\downarrow}| = 0.5$ are shown in curve *c*.

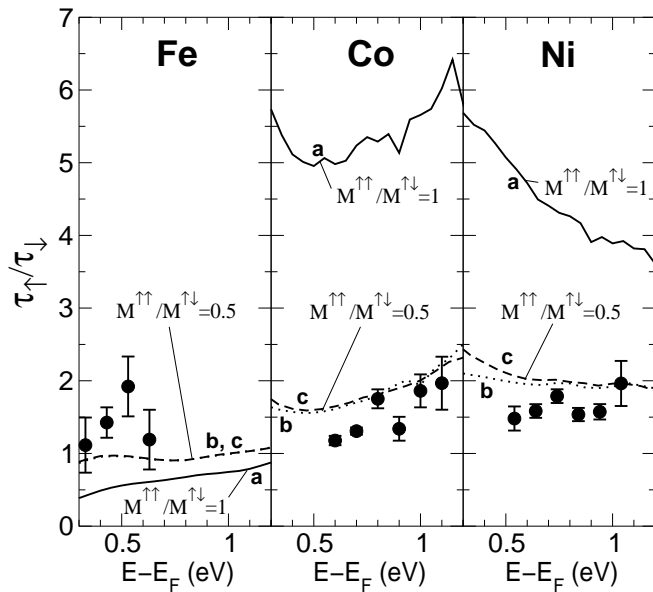


FIG. 10. Experimental and theoretical results for the ratio $\tau_\uparrow/\tau_\downarrow$ of the relaxation time of the distribution. The labels are as in Fig. 9 and refer to the same parameters.